



Norwegian University of
Science and Technology

Design of membrane energy exchanger concerning pressure loss

Aurora Retterstøl

Master of Energy Use and Energy Planning

Submission date: June 2018

Supervisor: Hans Martin Mathisen, EPT

Co-supervisor: Liu Peng, EPT

Norwegian University of Science and Technology
Department of Energy and Process Engineering

EPT-M-2018-71

MASTER THESIS

for

Student Aurora Retterstøl

Spring 2018

*Design of membrane energy exchanger concerning pressure loss**Design av membranvarmeveksler med hensyn til trykktap***Background and objective***Design of membrane energy exchanger concerning pressure loss**Design av membranvarmeveksler med hensyn til trykktap***Background and objective**

Membrane energy exchanger (MEE) is a novel device which is invented to assist HVAC system to provide a satisfactory indoor temperature and moisture level with possibly lowest energy consumption. The exchanger with the newly developed membrane can recovery both heat and moisture. It exhibits some unique features compared to conventional heat-recovery-only heat exchanger. The MEE investigated in this work is a quasi-counter flow exchanger consisting of several channels separated by membranes. The membranes are flexible, so they need support or reinforcement to prevent them from deforming. This support cause an unwanted pressure penalty for the flow through the channels.

This master work will basically investigate the performance of different types of spacers. The candidate has to suggest different designs and to test these in laboratory experiments.

The work is a continuation of the candidate's Specialization Project.

The following tasks are to be considered:

1. Update the literature study and theory on membrane exchangers and on laminar flow dynamics that was done in the Specialization project.
2. Suggest designs for spacers based on the parametric analysis of the pressure drop calculation
3. Construct and test the different designs
4. Evaluate the results and conclude the possible optimal design considering recovered energy and pressure penalty in the MEE

-- ” --

Within 14 days of receiving the written text on the master thesis, the candidate shall submit a research plan for his project to the department.

When the thesis is evaluated, emphasis is put on processing of the results, and that they are presented in tabular and/or graphic form in a clear manner, and that they are analyzed carefully.

The thesis should be formulated as a research report with summary both in English and Norwegian, conclusion, literature references, table of contents etc. During the preparation of the text, the candidate should make an effort to produce a well-structured and easily readable report. In order to ease the evaluation of the thesis, it is important that the cross-references are correct. In the making of the report, strong emphasis should be placed on both a thorough discussion of the results and an orderly presentation.

The candidate is requested to initiate and keep close contact with his/her academic supervisor(s) throughout the working period. The candidate must follow the rules and regulations of NTNU as well as passive directions given by the Department of Energy and Process Engineering.

Risk assessment of the candidate's work shall be carried out according to the department's procedures. The risk assessment must be documented and included as part of the final report. Events related to the candidate's work adversely affecting the health, safety or security, must be documented and included as part of the final report. If the documentation on risk assessment represents a large number of pages, the full version is to be submitted electronically to the supervisor and an excerpt is included in the report.

Pursuant to “Regulations concerning the supplementary provisions to the technology study program/Master of Science” at NTNU §20, the Department reserves the permission to utilize all the results and data for teaching and research purposes as well as in future publications.

The final report is to be submitted digitally in DAIM. An executive summary of the thesis including title, student's name, supervisor's name, year, department name, and NTNU's logo and name, shall be submitted to the department as a separate pdf file. Based on an agreement with the supervisor, the final report and other material and documents may be given to the supervisor in digital format.

- Work to be done in lab (Water power lab, Fluids engineering lab, Thermal engineering lab)
 Field work

Department of Energy and Process Engineering, 15. January 2018



Hans Martin Mathisen
Academic Supervisor

Research Advisor:
Liu Peng

Preface

The Master thesis was conducted at the Department of Energy and Process Engineering at the Norwegian University of Science and Technology, Trondheim. The thesis represents 30 ECTS for the spring semester and is a continuous work conducted by the author during the fall. Further, the thesis foremost an experimental study, whereas theoretical calculations also have been conducted.

First off, I would like to thank my supervisor Prof. Hans Martin Mathisen for giving me the chance to explore this exciting field. I want to take the chance to thank him for guidance throughout the semester and giving me constrictive feedback.

Likewise, I would like to give a special thanks to my co-supervisor Postdoctoral Peng Liu for all the knowledge on the topic that he was willing to share with me. He has spent much time helping me understand the concept as well as guiding me when I was running into problems with my calculations and experimental testing.

Lastly, my gratitude goes to Lars Konrad Sørensen who built the experimental test rig for me. Thank you for being patient with me and for transforming my sketches into a feasible experimental test rig.

Aurora Retterstøl

Aurora Retterstøl, MSc. student
Trondheim, June 11th 2018

Abstract

The world is facing climate changes that will have great influence on the ecosystem if changes are not being made. The building sector accounts for a great share of the total energy use in Norway and has therefore the possibility of being significantly reduced. An effect of this is shown in the building regulations where the requirements are getting stricter. The requirements for the ventilation system are also getting more rigorous, and therefore the choices concerning the components selected in the AHU must be deliberately selected.

Compared to a conventional heat exchanger, a quasi-counter membrane energy exchanger can recover sensible and latent heat, whereas the efficiencies have been proven to be sufficient in cold climates. Beneficially, the MEE obtains freezing problems occurring at a lower temperature. To keep the membrane from moving, spacers are inserted into the channels, which will be retaining the channel height. However, the pressure drops for a MEE increases compare to a flat plate heat exchanger due to the use of spacers. Therefore, the present thesis executed a theoretical and experimental pressure drop investigation for the MEE and the spacers. The pressure drop was measured under isothermal conditions, whereas the heat and moisture transfer were neglected.

According to the evaluated spacers, six different spacers were inserted into a test rig, were the pressure drop was measured for different airflow rates. The experimental investigation included different dimensions of the mesh screens as well as varying corrugation pitches.

The results gave that the corrugation pitch of the spacers had little influence on the porosity, whereas the mesh dimensions seemed to affect the most. In addition, both corrugation pitch and porosity influenced the pressure drop. Yet, the dominating contributor ensuring the lowest pressure drop could not be obtained by the study conducted in this thesis. Further, the experimental pressure drops results showed great promises for the tested spacers. The most promising spacer obtained the lowest pressure drop of 52 Pa when the average velocity was 1 m/s through the counter flow area. In addition, the most promising spacer was also the most porous tested spacer.

According to other studies, the spacers showed great potential of reducing the pressure drop through spacer-filled channels. The airflow rates selected for evaluation were based on the lower pressure drop this would enhance. To obtain larger velocities inside the channels, experimental testing must be conducted for the respective airflow rates. However, the pressure drop seems to still enhance low pressure drops compared to other studies. Different geometries of the spacers were conducted, but the ability to keep the membrane steady and from deflection could not be obtained by the executed investigations.

When the pressure drop for the MEEs are being reduced to the approximate same values as for heat exchangers utilized in residential buildings and the efficiency has been proven to be significant in cold climates, the MEE has a great potential for substituting the conventional flat plate heat exchanger in AHUs.

Sammendrag

Verden står overfor klimaendringer som vil ha stor innflytelse på økosystemet dersom ikke drastiske endringer blir gjort. Byggesektoren står for en stor andel av det totale energiforbruket i Norge og har derfor potensial for å bli betydelig redusert. Et resultat av dette er gitt i bygningsreglene hvor kravene blir strengere. Kravene til ventilasjonssystemet blir også strengere, og derfor må valgene som tas angående hvilke komponenter som skal benyttes i aggregatet gjøres med forsiktighet.

Sammenlignet med en konvensjonell varmeveksler kan en MEE gjenvinne både følbare og latent varme i tillegg til at effektiviteten viste seg å være tilstrekkelig i kaldt klima i laboratoriet ved NTNU. Fordelaktig med MEE er at fryseproblemer oppstår ved en lavere temperatur. For å holde membranen stabil ble spacers satt inne i kanalene for å opprettholde kanalhøyden. Derimot var trykkfallet for MEE tilsynelatende for høyt til å kunne bli installert i et ventilasjonsaggregat. Det er grunnlaget til at denne oppgaven utførte trykkfallsberegninger samt laboratoriske forsøk for trykktapet for MEE og spacerne. Trykktapet var målt under isotermiske forhold, mens varme- og fuktgjennomgang ble neglisjert.

I henhold til de evaluerte spacerne, ble seks forskjellige spacerer satt inn i en testrigg, hvor trykkfallet ble målt for forskjellige luftstrømninger. Den eksperimentelle undersøkelsen inneholdt forskjellige dimensjoner av nettingene, i tillegg til varierende korrugeringsavstander.

Resultatene ga at korrugeringsavstandene til spacerne hadde liten innflytelse på porøsiteten, mens nettingsdimensjonene virket å ha mest påvirkning. I tillegg, begge korrugeringsavstandene og porøsiteten påvirket trykktapet. Likevel kunne ikke den dominerende bidragsyteren som sikret det laveste trykkfallet oppnås ved resultatene som ble funnet i denne oppgaven. De eksperimentelle trykkfallene viste seg å være lovende for de testede spacerne. Den mest lovende spaceren oppnådde det laveste trykktapet på 52 Pa når gjennomsnittshastigheten var 1 m/s gjennom motstrømningsområdet. Dette var også den mest porøse spaceren.

I følge andre studier viste spacerne et stort potensial for å redusere trykkfallet gjennom spacer-fylte kanaler. Luftstrømningene ble valgt på grunn av det lavere trykkfallet dette ville gi. For å oppnå større hastigheter inne i kanalene, må eksperimentell testing utføres for de respektive luftstrømmene. Imidlertid ser det ut som trykktapet fortsatt vil være lavt sammenlignet med andre studier. Forskjellige geometrier av spacerne ble evaluert, men dens evne til å holde membranen stabil og fra å bøye seg kunne ikke stadfestes ved de utførte målingene.

Når trykkfallet for MEE har blitt betydelig redusert til liknende verdier i varmevekslere som er benyttet i boliger, og effektiviteten har vist seg å være signifikant i kaldt klima, har MEE et stort potensial for å erstatte den konvensjonelle plate varmeveksleren i ventilasjonsaggregater.

Table of Contents

Preface	i
Abstract	iii
Sammendrag - Norwegian abstract	iv
List of Figures	ix
List of Tables	xi
Nomenclature	xiii
1 Introduction	1
1.1 Background	1
1.2 Membrane Energy Exchanger	3
1.3 Objective	6
1.4 Assumptions	7
1.5 Method	8
2 Literature study	9
2.1 Pressure drop and effectiveness according to the exchanger structure	9
2.2 Pressure drop caused by polymer membrane	11
2.3 Evaluation of previous tested spacers	12
2.4 Pressure drops regarding other exchangers	14
3 Theory	15
3.1 Internal flow	15
3.1.1 Hydraulic diameter	15
3.1.2 Steady and unsteady state	16
3.1.3 Reynolds number	17
3.1.4 Entrance region in a channel	19
3.2 Pressure drop	20
3.2.1 Pressure	20
3.2.2 Pressure drop and representable equations	20
4 Modelling of spacer geometry and pressure drop	23
4.1 Geometries applied to the spacers inserted into the MEE	23
4.1.1 Ramp spacer	23
4.1.2 Sinusoidal spacer	24
4.2 Equations to calculate porosity	25
4.3 Pressure drop equation utilized in calculations	28
4.4 Pressure drop comparison	29
4.4.1 Friction factor correlation	29
4.4.2 Pressure drop correlation to previous study at NTNU	30

5	Experimental setup and planned experiments	31
5.1	Construction of the quasi-counter MEE	31
5.1.1	Exchanger structure	31
5.1.2	Corrugated mesh screen	34
5.1.3	Membrane	38
5.2	Experimental Facilities	38
5.3	Measurement schedule and execution	40
5.4	Uncertainty	41
6	Evaluation of the experimental test rig and conducted testing	43
6.1	Evaluation of test rig	43
6.2	Evaluation of the spacers	44
6.3	Evaluation of the testing	45
7	Theoretical and experimental results	47
7.1	Results of theoretical calculations	47
7.1.1	Porosity	47
7.1.2	Calculated pressure drop	48
7.2	Experimental testing	51
7.2.1	The average pressure drop results	51
7.2.2	The pressure drop concerning the pressure taps	52
7.3	Pressure drop according this and other studies	55
7.3.1	Friction factor regarding experimental testing	55
7.3.2	Pressure drop correlation to other studies	57
7.3.3	Friction factor according to other studies	58
8	Comparison and discussion of results	59
8.1	Investigation of theoretical and experimental pressure drop	59
8.2	Comparison and discussion of the experimental testing	60
8.2.1	Different conducted tests	61
8.2.2	Pressure taps	63
8.2.3	Transition to turbulence due to filament	66
8.3	Pressure drop comparison to other studies	67
9	Conclusions	69
10	Further work	71
	Appendices	77
A	Hazard activity identification process	A-1
B	Minor loss coefficients	B-1
C	MATLAB-script used in theoretical pressure drop calculations	C-1
D	Results of the inlet demonstration	D-1
E	Specific values for the created moulds	E-1
F	Specific values for the measurement schedule	F-1

G	Parameters obtained by the porosity calculation of the corrugated mesh screens	G-1
H	Pressure drop theoretical calculation	H-1
I	Results of the pressure drop from actual experiments	I-1

List of Figures

1.1	The working principle of the Quasi-counter exchanger	4
1.2	The cross flow structure as considered in this thesis	4
1.3	Empty channels stacked on top of each other at a cross flow edge	5
2.1	Design of quasi-counter flat plate heat exchanger; (a) pressure drop and (b) effectiveness as a function of flow rate	10
2.2	Spacer geometries investigated in Woods and Kozubal's study	12
3.1	Flow behaviors around a cylinder for various regimes as the Reynolds number increases	18
4.1	Structure of ramp geometry	24
4.2	Structure of sine curve	24
4.3	Description of the different directions in the exchanger	26
4.4	Description of the different directions in the exchanger	28
5.1	The exchanger channels with named pressure taps and channels	32
5.2	The inlet demo and testing procedure	33
5.3	Detailed description of the inlet/outlet part	34
5.4	The general spacer structure with sinusoidal geometry	34
5.5	The mould imprint and the cross-sectional view of Mould 1 and 2	36
5.6	Example of the two different periods for the corrugated mesh screens	37
5.7	Schematic representation of the experimental test rig	38
5.8	Pressure taps located before the effective exchanger area	40
6.1	The test rig, showing the setup of instruments and pressure tubes.	44
6.2	Plastic film rupture and measures to avoid the occurrence	46
7.1	The calculated porosity of the conducted experimental tests. Same colors express same mesh screen.	48
7.2	Theoretical pressure drop for ramp and sinusoidal geometry of the spacer for an airflow rate of 30 L/min	49
7.3	Theoretical pressure drop for triangle and sinusoidal geometry of the spacer for the chosen periods	50
7.4	The experimental results for the average pressure drop	51
7.5	The friction factor dependent on the Reynolds number	55
7.6	Friction factor comparison to Woods and Kozubal's research	58
8.1	The calculated porosity and experientnal pressure drop respective to the tested spacers for 30 L/min. Same colors express same mesh screen.	61

D.1	Location of the different measuring points	D-1
I.1	Notation of pressure taps in the exchanger	I-2

List of Tables

3.1	The range of Reynolds number for the different flow regimes in pipes . . .	17
3.2	Minor losses applied to the pressure drop calculations	22
5.1	Specific physical properties for the exchanger casing	33
5.2	Specific properties of the meshes	35
5.3	Specific properties of the corrugated spacers	37
5.4	Summary of which mould and mesh utilized in the different experimental tests	40
7.1	Calculating the pressure drop according to stated values in the study conducted by P. Liu	57
7.2	The pressure drop according to Test 4 comparable to the study conducted by P. Liu	57
B.1	Minor loss values for rectangular bend in ventilation ducts	B-1
D.1	Velocity and standard deviation for the chosen diffusion pieces at the end of the inlet area	D-1
E.1	Specific properties of the moulds	E-1
F.1	Specific values for the measurement schedule	F-1
G.1	Parameters needed to calculate the porosity of the corrugated mesh screens	G-1
H.1	Theoretical pressure drop calculated for the different geometries	H-1
H.2	Theoretical pressure drop calculated for the different geometries at 30 L/min	H-1
H.3	Theoretical pressure drop for the different geometries according to a corrugation pitch of 10 L/min	H-2
H.4	Theoretical pressure drop for the different geometries according to a corrugation pitch of 20 L/min	H-2
I.1	The average pressure drop for the exchanger for the different conducted tests	I-1
I.2	The pressure drop according to the different pressure taps for Test 0. The average pressure drop for different measurements are also given	I-3
I.3	The pressure drop according to the different pressure taps for Test 1. The average pressure drop for different measurements are also given	I-5
I.4	The pressure drop according to the different pressure taps for Test 2. The average pressure drop for different measurements are also given	I-5
I.5	The pressure drop according to the different pressure taps for Test 3. The average pressure drop for different measurements are also given	I-6
I.6	The pressure drop according to the different pressure taps for Test 4. The average pressure drop for different measurements are also given	I-6
I.7	The pressure drop according to the different pressure taps for Test 5. The average pressure drop for different measurements are also given	I-7

I.8 The pressure drop according to the different pressure taps for Test 6. The average pressure drop for different measurements are also given I-7

Nomenclature

Abbreviations

AHU	Air handling unit
ASHRAE	American Society of Heating and Air-Conditioning Engineers
CFD	Computational Fluid Dynamics
ERV	Energy recovery ventilator
HRV	Heat recovery ventilator
IAQ	Indoor air quality
MEE	Membrane energy exchanger
RH	Relative humidity
SFP	Specific fan power
TEK	Building technical regulation
VOC	Volatile organic compound

Parameters

A	Area	m^2
a	Half of corrugated pitch	m
b	Half of wave height	m
D	Diameter	m
d	Equilibrium line	
f	Friction factor	Pa
G	Specific mass flow rate	kg/m^2s
g_c	Proportionality constant in Newton's second law of motion, $g_c = 1$	
H	Channel height	m
k	Function repetition	
$K_{L,\infty}$	Incremental pressure drop coefficient for fully developed flow	
L	Length	m
n	Number of waves	

P	Period, Pressure	m,Pa
p	Perimeter	m
Re	Reynolds number	
V	Velocity	m/s
W	Channel width	m

Greek symbols

α	Angle	
α^*	Area change for a wave	
λ	Wavelength	m
μ	Fluid viscosity	kg/ms
ρ	Density	kg/m ³
σ	Porosity	
τ_w	Shear stress at the wall	N/m ²
Θ	Angle of the cross flow section	
φ	Phase shift	

Sub- and superscripts

avg	Average
c	Cross-section/constant
D	Darcy
e	Exit
fd	Fully developed
h	Hydraulic
i	Start, given value, inner
j	End
L	Losses
o	Outer
w	Wall

Chapter 1

Introduction

This chapter states the background for the thesis and explains the concept of the membrane energy exchanger. The next sections are continuous work from the project work done by the author during fall semester 2017 [1]. Further, the objectives, assumptions and method conducted for the present thesis will be given.

1.1 Background

The climate changes that are occurring is predicted to be human made as well as having irreversible impacts on the ecosystem if the emissions of the greenhouse gasses are not drastically reduced [2]. Accordingly, the building sector has been reducing the climate footprint by implementing stricter regulations which has led to decrease in energy usage in buildings. However, the building sector in Norway stands for approximately 40 % of the total energy use [3] and has a great potential for being further reduced.

The technical regulation for buildings in Norway, hereby referred to as TEK, has become more rigorous over the years. It is therefore important to choose energy efficient technical equipment as well as high performance building body. Further, the latest building regulation, TEK 17, has strict requirements for the ventilation system. The heat recovery has to be of minimum 80 % efficiency while the specific fan power (SFP) cannot exceed 1.5 kW/m³/h [4]. Given these values, the regulation demands higher quality and performance of the air handling unit (AHU). Thus, the components in the AHU should not contribute to a higher pressure losses to ensure sufficient performance when the increase introduce a larger fan power need.

It is a known problem that during cold winters the indoor air can feel dry and increase the unsatisfied share of the occupants. Dry air can increase irritation of the eyes and upper airways. Therefore, the optimal indoor relative humidity (RH) is determined to be between 25 ~ 40 % RH during the winter. [5] However, indoor dissatisfaction can come from dry indoor air which is stated to be influenced by indoor air pollutant rather than the air humidity [6]. Wolkoff and Kjærgaard [7] concluded that the mentioned statement above of indoor pollutants being the reason for dry air and poor indoor air quality (IAQ) rather than RH should be reconsidered. This was due to the complexity of influences by RH combined with pollutants like ozone and VOCs that have been lacking research. Further research on the field was not possible to allocate.

To assure good indoor environment for occupants, ventilation plays a key role. It is therefore important to choose components for the AHU that is appropriate for the local outdoor conditions as well as the type of building. Further, to establish good IAQ and given the prediction of stricter requirements for the energy efficiency according to the heat exchangers, the solution might be a novel heat/energy exchanger.

A commonly used heat exchanger is the flat plate heat exchanger. Beneficially, it does not transfer pollutants from the exhaust air to the fresh inlet air, being a recuperative heat exchanger. Additionally, the exchanger consists of non-moving parts and has therefore been considered to be durable. Although, the heat recovery efficiency is relatively low compared to the regulation requirement and the exchanger has freezing problems. Freezing occurs when the hot and humid air in the exhaust duct reaches the dew point temperature and the water vapor condensate. When the outdoor temperature is low enough, the condensed water will freeze. That is an unwanted occurrence and a common practice today is to use freeze protection methods in AHUs. These methods increase the energy use and additionally lower the overall efficiency for the heat exchanger. [3, 8]

Further, the conventional flat plate heat exchanger can be converted to an energy exchanger which recovers moisture and heat through layers of membrane sheets. In addition, the efficiencies have been proven to be sufficient. [9] Due to the favourable efficiencies and other benefits that will be described in the next section, the energy exchangers could be replacing the conventional heat exchangers that are utilized today. Respectively, that is why this thesis will be focusing on this type of exchanger.

1.2 Membrane Energy Exchanger

Even though the membrane energy exchangers (MEE) can be a new subject for many, T. Osamu [10] first introduced the concept in 1969 when he changed the surface of a flat plate heat exchanger with a water-permeable paper sheets. Later, polymer membranes replaced the paper sheets due to having a dense pore structure, being more durable and easier to install [11]. Thus, the membrane was more reliable for ventilation purposes.

A MEE is one type of energy recovery ventilator (ERV) that exchanges both latent (moisture) and sensible (heat) heat [9]. The energy transfer is occurring due to difference in temperature and moisture of the supply and exhaust air which are located on opposite sides of the membrane. Appropriately to the disparity in temperature, the sensible heat is transferred by convection when the heat conduction is negligible due to the small thickness of the membrane. [12] Further, the transfer of moisture, or latent heat, is a result of diffusion of water vapour through the pores in the membrane [13]. According to J. Woods [13], the amount of water vapor will depend on the pore structure and thereby the permeation rate.

According to several studies, the MEE provides great sensible and latent effectiveness which can be greater than other conventional heat exchangers. Thus, the MEE provides energy saving potential that will result in less need of additional energy for heating or cooling dependent on the purpose of the device. Accordingly, the IAQ can be improved due to moisture recovery that will benefit the exchanger for being further installed into AHUs. [9, 13–15]

The exchanger can be conducted in different shapes which will influence the efficiencies. A cross flow exchanger is assembled in a manner that the airflows are crossing each other in the different air channels. This design makes it easier to place the exchanger in an AHU when the inlet and outlet for the different flows are located at different sides of the exchanger. However, the efficiency is not as good as for a counter flow exchanger. [13] The counter flow exchanger has the two airflows flowing in opposite directions. Despite the satisfying effectiveness, the construction of the exchanger in an AHU would not be beneficial due to the location of flows and would therefore be hard to implement [16]. Thus, a quasi-counter exchanger utilizing both cross and counter flow arrangement obtaining good efficiencies and will further be evaluated in this project.

Further, L. Z. Zhang [9] conducted a simulation study to investigate the quasi-counter arrangement. The conclusion stated that the counter flow area should be the dominating area in the exchanger and reduce the cross flow area. However, regarding the cross flow area, the arrangements are necessary when connecting the ductwork to the exchanger. Therefore, the connections between the exchanger and duct should be thoroughly designed. The working principle of the quasi-counter exchanger is shown in figure 1.1.

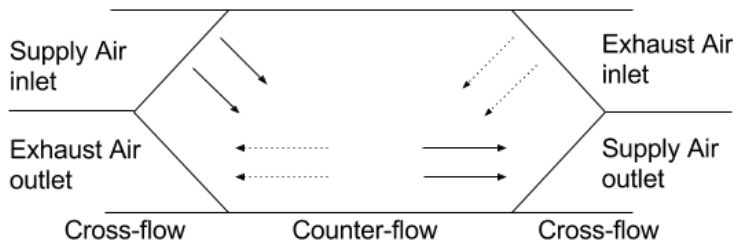


Figure 1.1: The working principle of the Quasi-counter exchanger

As shown in figure 1.1, the supply air enters the cross flow area and continues through the counter flow part before leaving the exchanger through the last cross flow area, as the solid lines indicate. The exhaust air is given by the dotted lines and follows the same flow pattern as the supply air, although in separate channels located above and below the viewed channel for supply air.

The MEE uses sheets of membrane to keep the fresh outdoor air separated from the polluted exhaust air. The membrane is usually divided into two categories, dense and porous, which depends on the pore structure. The pores vary from the order of 1 nm to 1 μm respectively for the two categories. These categories utilize different mechanisms to diffuse water vapor through the membrane. Further, the most commonly used membrane in ERVs has dense pore structure due to the strong affinity to water. [13]

However, to ensure good IAQ the membrane must be permeable to water vapour rather than other pollutants existing in the air. That will reduce the risk of pollutant transferring between the airflows. [13] Despite the studies [17, 18] showing an adequate selectivity of water vapor, it should not be excluded that pollutants can transfer between the airflows according to J. Woods [13]. The pollutant transfer should therefore be evaluated in an actual ventilation system to ensure proper IAQ yet the chances are marginal.

Supplementary, the quasi-counter arrangement consists of two cross flow areas. The geometry of these two parts will be identical, but with mirrored orientation. When investigating the areas, the structure can be considered as a rhombus or a square, dependent on the angle. Figure 1.2 shows the cross flow area considered as a square in the thesis due to the angle, θ , of 45°. For all other angles, the geometry would be a rhombus.

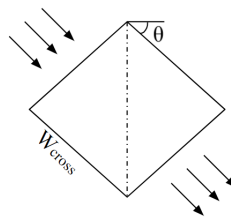


Figure 1.2: The cross flow structure as considered in this thesis

The flat plate quasi-counter energy exchanger is conducted by channels located above each other where the airflows are separated by membrane sheets, as stated. Figure 1.3 shows how the stacked channels are located at the inlet/outlet of the exchanger (at the cross area). As the figure shows, when air enters at one channel stack, there is no air leaving at the same side of the stack. The white channel represents an opening for either entering or exiting airflows and the grey area is the representative channel wall.

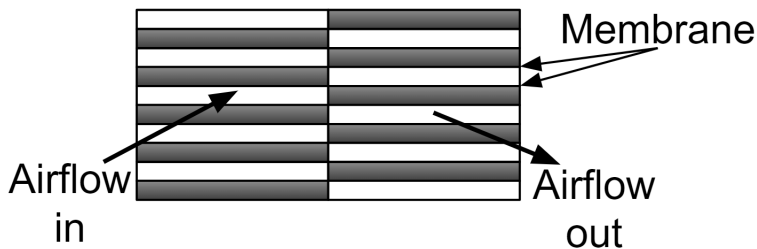


Figure 1.3: Empty channels stacked on top of each other at a cross flow edge

Moreover, the research that has previously been conducted on the topic of MEE has mostly been considered for warmer climates, where the membrane dehumidifies and cools the supply air. When a MEE has been used for air conditioning, the latent and moisture efficiencies have been proven to be significant. [15, 19] Accordingly, the total efficiency for a MEE compared to conventional heat exchanger utilized for air-conditioning purposes were great. However, the total efficiency had a smaller increase when the MEE was used for heating purposes. [13] Although, the study did not consider the effect of condensation in the exhaust air duct for low outdoor temperatures. This could benefit the overall efficiency for the MEE compared to heat recovery ventilators (HRV) if freezing would occur, which is given below.

The research on the MEE for cold climates is limited. Although, for the research [20] that has been studying the effectiveness in cold climates gives great promise for the exchanger. When both heat and moisture are being recovered, the freezing point in the exchanger is being reduced to a lower temperature. This is due to the reduced humidity in the exhaust air making it more adaptable for cold climates. Thus, the energy savings can be of significance since the reduced use of frost protection in a ventilation system. The energy required for heating will also be diminished when the thermal efficiency could be better than for conventional heat exchanger.

Despite the promising effectiveness of the MEE, the study conducted by P. Liu [21] testing the MEE in cold climate obtained a large pressure drop that is undesirable for future exchangers in Norwegian ventilation systems. The MEE needs spacers to keep the membrane sheets apart, due to deflection when becoming wet, which will introduce an increase in the pressure drop. Thus, the spacers have great potential for improving the design to reduce the pressure drop.

1.3 Objective

As stated above, the MEE has shown great potential to achieve considerable effectiveness for sensible and latent heat. However, due to strict requirements for AHU components in TEK, the pressure drop according to the MEE is in the interest of being reduced. The spacers and membrane in the MEE can impose a great pressure drop and will therefore be evaluated in this thesis.

The present thesis will study the pressure drop according to exchanger casing and spacers and their ability to keep the membrane steady by theoretical calculations and experimental investigations. Further, the objectives in this thesis which will be evaluated, are stated below.

- Sketch and construct the exchanger casing in a manner where spacers easily can be experimentally tested and substituted. The exchanger casing should also contribute to the lowest possible pressure drop.
- Determine spacer geometries and size of corrugation pitches based on theoretical calculations and the construction ability. Thus, moulds according to the decisions have to be created in accordance to the chosen mesh screen to achieve the desired results.
- Build the test rig and construct the different spacers that will undergo experimental testing. Evaluate the different spacers based on the pressure drop and ability to keep the membrane steady at different airflow rates.

1.4 Assumptions

Assumptions that have been made in the pressure drop calculations and the experimental testing are stated below. The assumptions are made on the basis of making minor mistakes while doing the theoretical calculations and accordingly the experimental testing.

According to the calculations, the flow will be handled as laminar flow in steady state condition. The properties of the flow are set to be steady, when in reality it would be changing according to outdoor conditions. Another assumption is that the spacers are considered to have no thickness, whereas this would complicate the calculations. Also, in the calculations, the spacer shape in the cross flow area is assumed to be following the shape of the channel, hence changing directions through the exchanger. This was not conducted for the experimental testing, but was applied to simplify the calculations.

The concern for the membrane to still deflect even though a spacer is applied is not included in the calculations. The flexibility of the membrane could contribute to further blockage of the air through the channel and increase the pressure drop. Although, the effect was not considered in the calculations. The effect would have had to be evaluate by simulation models.

According the calculation of the porosity, the woven mesh was assumed to be flat. However, at the crossings, the wire would double. It is assumed that this fraction is the same for all corrugation meshes and would not affect the difference in porosity amongst the investigated mesh screens. Further, the calculations were conducted for solid surface spacers, whereas the experimental spacers were made of mesh screens. Due to complicated calculations for the mesh screen, it was excluded from the evaluation. The theoretical calculations were foremost used for interpretation of the pressure drop reduction according to different geometries and corrugation pitches and was therefore assumed to be appropriate.

For the experimental investigation, it has been assumed that only the statical pressure was measured at the pressure taps. During measurements, the exchanger was standing, and the pressure taps would be located at different elevations. However, the difference in heights regarding the respective taps were about 125 mm and the hydrostatic pressure drop was therefore neglected. It has also been assumed that the dynamic pressure did not influence the pressure measurements but was investigated to ensure results.

1.5 Method

This chapter states the methodology that has been used to evaluate the pressure drop occurring due to the different designs of the spacers. The exchanger that was studied was a quasi-counter membrane energy exchanger where the flow was laminar and in steady state conditions.

The thesis is a continuous work accomplished by the author where the main focus was to calculate the pressure drop in a MEE with and without corrugated spacers [1]. Different geometric shapes and corrugation pitches of the spacers were investigated. Also, a sensitivity analysis was conducted to evaluate how the pressure drop was affected when varying counter width and length, channel height, number of periods for the spacers and lastly the airflow rate. The results made the basis for selections of the spacers that have been investigated in this thesis.

To further understand the topic of the MEE, available literature was investigated to get a better understanding of the field and the research done before. To find appropriate information, different web-based database such as *Knovel*, *ScienceDirect*, *Researchgate* and *Google Scholar* were much used as well as relevant textbooks.

In accordance with the supervisors and laboratory staff, sketches of the exchanger and moulds to create the spacers were created before being constructed in the laboratory. The exchanger casing and moulds were drawn in AutoCADs Inventor by the laboratory staff and was carved out by a CNC milling machine at NTNU. A hazard activity identification process sheet were created to clarify hazardous activities and measures to avoid them, which can be found in Appendix A. The previous developed calculation setup for pressure drop [1] was improved and modified to fit the current case. Microsoft Excel was mainly used due to the ease of making changes to the calculations, whereas MATLAB was only used for calculation of the sinusoidal cross-sectional area.

When the exchanger and spacers were constructed, the test rig was assembled. An extensive research for the statical pressure was conducted according to multiple taps located perpendicular to the exchanger walls. Further, the pressure drops regarding the channels and average pressure drop for the exchanger could be evaluated.

A comparison of the constructed spacers was executed to be able to evaluate the performance of the different spacers. Accordingly, the experimental results regarding the spacers were compared to literature stated in the section 2.

Literature study

To get a better understanding of the correlation between the MEE and pressure drop, previous work of the field has been studied and stated below. It is also trivial to consider the relation between the pressure drop and effectiveness when designing an exchanger, since decisions can not be made on the basis on only one of them. The literary study is a continuous work from the project work done by the author during fall semester 2017 [1], with more depth on representative pressure drop.

As previously mentioned, the quasi-counter MEE has achieved good efficiencies for both latent and sensible heat including the MEE conducted by P. Liu [20]. P. Liu stated that the exchanger arrangement could be an ideal alternative compared to the cross flow heat exchangers that have been widely used for conventional HRV, also in cold climates. Yet, he attained a large pressure drop through the spacer-filled channels. Thus, the pressure drop was in interest of being reduced while maintaining the satisfying effectiveness.

2.1 Pressure drop and effectiveness according to the exchanger structure

There are different parameters influencing the pressure drop in a quasi-counter exchanger, and firstly the exchanger structure will be considered. The dimensions of the exchanger arrangement will affect both the effectiveness and pressure loss. A common knowledge is that there might be a trade-off when choosing good effectiveness which will induce a large pressure drop as well. Previous studies encountering this topic for the relevant exchanger arrangement are given below.

V. Dvořák and T. Vít [22] conducted a numerical study where the thermal effectiveness and pressure drop were evaluated for different dimensions of a quasi-counter flat plate heat exchanger. In the study, the exchanger's total length and the volume was kept constant, whereas a combination of four different exchanger widths and heights were evaluated. The results were summarized in graphs which are given in figure 2.1. In the figure, the evaluated arrangements are given to the left and the pressure drop and effectiveness for the specific arrangements are located to the right respectively.

Considering the graph regarding the pressure drop in figure 2.1, the counter flow arrangement that is wider than longer (grey line - 0.4×0.15) gives the lowest drop. Accordingly, this arrangement gives the lowest effectiveness. The opposite goes for the arrangements that have a counter flow area that are longer and thinner. When the arrangement has the longest counter flow area the pressure drop is fairly reduced (blue line - 0.15×0.4) while maintaining the highest effectiveness compared to the second longest arrangement (orange line - 0.2×0.3) that obtained a larger pressure drop. [22]

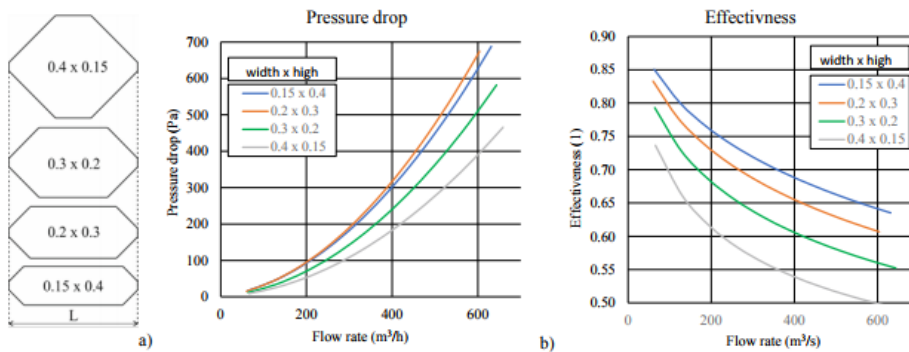


Figure 2.1: Design of quasi-counter flat plate heat exchanger; (a) pressure drop and (b) effectiveness as a function of flow rate (reprinted with permission [22])

Moreover, the flow attack angle, describing the angle of the air entering the exchanger channels, affects the effectiveness and pressure loss. R. Al-Waked et al. [23] created a CFD-simulation that evaluated the latent and sensible effectiveness and accordingly the pressure drop when supply and exhaust air entered the cross flow area in various directions. The result gave the greatest sensible and latent effectiveness when the entering air encountered the cross-sectional area perpendicular. Concerning the pressure drop, the same attack angle did not however, encourage the lowest loss. To ensure the lowest pressure drop, the airflows would enter the exchanger so that no directional flow changes would occur inside the exchanger. Although, the situation was clearly not favourable for the effectiveness. Lastly, the air could enter at a 45° angle to the inlet area which did not introduced the largest pressure drop nor effectiveness. Therefore, the study concluded that the perpendicular inlet flow would be the most suitable solution to achieve the best airflow performance.

Woods and Kozubal [24] conducted a study where they investigated different types of spacers, and the respective efficiencies and friction factors. They also evaluated the friction according to the laminar flow for the empty channel. The results gave an experimental friction factor for the open channel that was in the range of 1-8% higher than the laminar theory. For larger Reynolds numbers the experimental friction factor was increasingly differentiated from the theory. They stated that it occurred due to the irregularities in the surface when larger Re is gradually being more dependent on the surface roughness.

2.2 Pressure drop caused by polymer membrane

The difference between the flat plate heat exchanger and energy exchanger, is the sheets of membrane that separates the airflows which introduces moisture transfer as well as heat. However, the membrane itself can impose an additional pressure drop. The polymer sheets are elastic and can deflect due to differential air pressure across the membrane and pre-slacking during manufacturing of the exchanger. [13] M. D. Larson et al. [25] conducted a research on how the pressure drop was affected by pre-stressed membranes with channel support such as spacers. They concluded that air-to-air exchangers should not be manufactured with slack membranes due to the contribution of a large air flow resistance when deflecting. Even though the membrane would be pre-tightened, a good structural scheme may be required to avoid further deflection and to retain a uniform channel height.

Further, Larson et al. [25] evaluated the membrane deflections into the air channels. The mass flow rate over the channels were assumed to be identical. Further, the flow channels achieving the positive pressure, the membrane would deflect out outwards, whereas the negative pressure flow channel would have the membrane deflection into the channel. Thus, when the membrane was not pre-stressed, the negative pressure channel would obtain larger pressure drop than the positive channel.

Another study conducted by Y. Lu et al. [26] replaced the fixed plates in a cross flow HRV with plastic film. The film did not introduce moisture recovering, but induced vibration on the film by the airflow which enhanced a good latent efficiency. However, the film vibration would change the channel height which would introduce a larger flow resistance. By the use of thin films, the intensity of the film vibration increased compared to thicker films for the same airflow rate, which resulted in larger channel deformation.

2.3 Evaluation of previous tested spacers

As well as the exchanger arrangements affects the pressure drop and effectiveness, the spacer will also have a great influence on both areas. As mentioned, J. Woods and E. Kozubal [24] conducted a study for laminar flow testing different types of spacers. The shapes of the different corrugated spacers were solid triangle spacer and two porous sinusoidal spacers. The investigated spacers are shown in figure 2.2. Their experimental testing gave that the solid triangle spacer (**a**) reduced the heat transfer if the material was of low conductivity and regardless conductivity mass transfer would be reduced. Importantly, the pressure drop was greatly increased compared to an empty channel.

Further, the study stated that the mesh spacers (**b** and **c**) gave better heat efficiencies and a fairly increase in mass transfer efficiencies. The pressure drop was moderately increased compared to channels with no spacers. For one of the mesh spacers (**c**), the orientation of the air flowing through the spacer, previously given as the attack angle, varied between 0° , 45° and 90° . The flow orientation for 0° gave the lowest friction factor compared to orientations of 45° and 90° . Overall, when considering both pressure drop and effectiveness, mesh spacers imposed the greatest abilities. The porosities obtained for the spacers were given to be 0.89, 0.95 and 0.98 according to spacer **a**, **b** and **c** respectively.

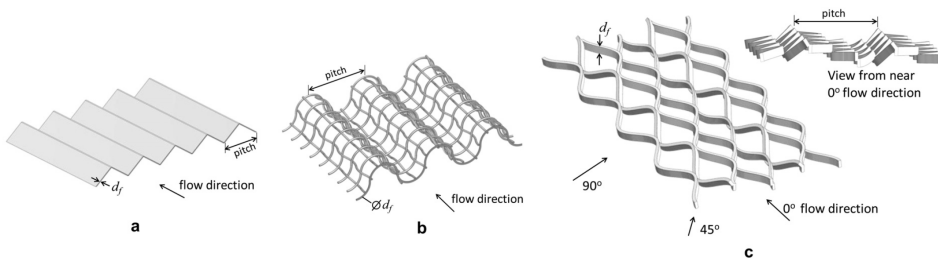


Figure 2.2: Spacer geometries investigated in Woods and Kozubal's [24] study (reprinted with permission [24])

Continuously, the experimental friction factor considering all of the mesh spacers obtained by Woods and Kozubal [24] deviated from the theory for Re larger than 500. The authors stated it was likely caused by the flow entering the transitioned regime of unsteady flow due to a filament-based Reynolds number, Re_f . Thus, the flow was likely affected by the presence of the filament walls. Further, the experience of the steady flow becoming unsteady when the flow rate increases, have been observed by other researchers for liquid flows. For a laminar liquid flow in a channel, an obstacle can construct a local transition to the turbulent regime, commonly by vortices being created behind the obstacle. However, this depends on the shape of the obstacle, height of the channel and the properties of the flow whether turbulence will occur. [27]

There have been done a larger research on membrane-based channels for liquid flows, such as water desalination, water reclamation and product treatment, concerning the pressure drop due to spacers. Commonly used spacers are flat mesh spacers filling the height of the channel or a zigzag spacer which is more like the once relevant for the present thesis. The spacers are mainly inserted to keep the membrane apart but are also used to introduce mixing of the flow. In addition, the zigzag spacer did not introduce the lowest pressure drop. The zigzag pattern was located transverse to the flow direction, meaning the flow had to undergo directional changes creating a larger pressure drop. However, that is a wanted scenario for these research papers. [28–34] Further, some of the studies [28–31] concluded that the filament diameter and the angle between the filament greatly affected the pressure drop.

Santos et al. [35] conducted experimental and numerical testing of 12 different flow-aligned (not corrugated) spacers. They observed the transition from laminar to turbulent flow, dependent on the spacers, for increasing Re . The filament was investigated, and they saw that the different directions (transverse and longitudinal) had different impacts on the pressure drop. The transverse filaments were the contribution factor according to the friction creating form drag. The longitudinal filaments were shown to less effected on the pressure drop, contributing with viscous drag on the surface. They also stated that the friction factor would increase by the increase of transverse filaments per unit length.

As mentioned above, the spacers have been introduced as flow mixers for liquid flows. However, this can also be the case for air-to-air heat exchangers. In an experimental study done by G. I. Mahmood et al. [36], the pressure drop and heat transfer were investigated over varying Reynolds numbers in a cross flow heat exchanger. The Reynolds numbers were chosen in the range of the transition regime. They inserted a sinusoidal porous screen into a rectangular channel to introduce better mixing of the flow and temperature. The results showed that the heat transfer increased according to the Reynolds number but accordingly did the pressure drop. When the Reynolds number were in the upper region of transition regime, the friction factor reduced due to more turbulent flow.

Further, it seems like little research of the porosity according to the spacers affecting the pressure drops are minimal concerning the MEE and also for liquid-based equipment. Sid-diqui et al. [37] conducted a numerical experiment testing various porosity measurement methods for different feed spacers for a spiral-wound membrane system. The porosity among other factors differed for the different spacers. They concluded that pressure drop was super linearly dependent on the porosity. Thus, the pressure drop could be reduced significantly when the porosity of the spacer would be increased.

2.4 Pressure drops regarding other exchangers

Pressure drops according to other relevant studies have been examined to be able to evaluate the results conducted in this thesis. Accordingly, it is interesting to evaluate what commercial flat plate heat exchangers obtain of pressure drop.

Flat plate heat exchangers have utilized for a long time and for fixed plate exchangers the minimum pressure drop was given to be 100 Pa. In this case, the pressure drop was not differentiated between counter- and cross flow arrangements. [38] However, the study conducted by Y. Lu et al. [26] which was stated earlier, conducted an experiment where they replaced fixed plates in a cross flow HRV with plastic film. The exchanger achieved a pressure drop as low as maximum 20 Pa for the tested airflow rates. The average velocity was calculated to be 1 m/s according to the stated values, which gave the pressure drop of between 4.5 to 6 Pa regarding the different film thicknesses. Additionally, they did not insert any structural support into the channels.

Regarding the pressure drop range for an energy exchanger have been found to be between 100 and 500 Pa [38]. It is said that if the pressure drop for an exchanger would exceed 350 Pa is it unlikely to be installed in an AHU due to the increased need of fan power [13]. Danfoss [39] has obtained their reference pressure difference to be of 50 Pa through the AHU. They have incorporated a flat plate heat exchanger with the quasi-counter arrangement, whereas the pressure drop over the exchanger will be somewhat smaller than 50 Pa.

A previous stated research was conducted at NTNU, whereas P. Liu [40] encountered a significant large pressure drop when conducting experiments of a quasi-counter exchanger. According to his study he obtained a pressure drop of 524 Pa when the average velocity in counter flow part obtained a value of 1.56 m/s.

According to the literature research stated above, when selecting a spacer and the exchanger structure for the MEE, it will have a significant impact of the latent and sensible effectiveness and as importantly the pressure drop. Accordingly, the spacer and structure must carefully be decided not to greatly increase the pressure drop making the MEE not applicable for the market.

Chapter 3

Theory

In this chapter, theoretical relations relevant to the MEE are given. That includes the relations for internal flows and the pressure drop. Required definitions and equations are given to be able to complete theoretical and experimental pressure drop evaluations. This chapter is also a continues work conducted by the author during the fall semester [1].

The spacer geometries that were evaluated in the present thesis were sinusoidal and rectangular geometry, where relevant equations according to the pressure drop calculations amongst others are stated below. The rectangle represents a ramp like geometry but will be further explained in section 4.1.1.

3.1 Internal flow

When considering a membrane energy exchanger, the airflows will be considered as internal flows due to flowing through channels. For the particular case, the channels consist of flat plates stacked on top of each other.

3.1.1 Hydraulic diameter

For non-circular pipes or channels, the dimension of hydraulic diameter is commonly used when considering dimensionless quantities. The hydraulic diameter is reduced to the circular pipe diameter, making the value comparable for different geometries. The definition of the hydraulic diameter, D_h is given in equation 3.1. As the equation states, it is dependent on the wetted cross-sectional area and perimeter which makes it reliant on the amount for fluid inside the channel or pipe. [41]

$$D_h \equiv \frac{4 \times \text{Wetted cross sectional area}}{\text{Wetted perimeter}} = \frac{4A_c}{p} \quad (3.1)$$

The hydraulic diameters that are applied in the present thesis are given for the empty channel in equation 3.2 [41], whereas rectangular- and sinusoidal spacers are stated in equation 3.3 and 3.4 respectively [42].

$$D_{h, Channel} = \frac{2WH}{W + H} \quad (3.2)$$

$$D_{h, Rectangle} = \frac{4b}{1 + \alpha^*} \quad (3.3)$$

$$D_{h, Sinusoidal} = (1.0542 - 0.4670\alpha^* - 0.1180\alpha^{*2} + 0.1794\alpha^{*3} - 0.0436\alpha^{*4})2a\alpha^* \quad (3.4)$$

The relation of the height, $2b$, and the width of the corrugated pitch, $2a$, is represented by the ratio of α^* given in equation 3.5.

$$\alpha^* = \frac{2b}{2a} \quad (3.5)$$

For calculating the hydraulic diameter for the rectangular- and sinusoidal geometry, equation 3.3 and 3.4 respectively is valid when the ratio of α^* is within:

Rectangle $0 \leq \alpha^* \leq 1$

Sinusoidal $0 \leq \alpha^* \leq 2$

3.1.2 Steady and unsteady state

The state of the flow is determined by whether the conditions are in steady or unsteady state.

Steady state Time independent properties of the flow, meaning velocity and pressure to mention some at every point in the flow are autonomous of the time. According to the time independent properties, the average velocity can be calculated with the given formula in equation 3.6. [41]

$$V_{avg} = \frac{\dot{m}}{\rho A_c} \quad (3.6)$$

Further, the specific mass flow rate is stated in equation 3.7 which is used in some pressure drop relations [42].

$$G = \rho V_{avg} = \frac{\dot{m}}{WH} \quad (3.7)$$

Unsteady state The properties of a flow that is unsteady is time dependent at every point. This means that the properties are always changing and can increase the complexity of calculations compared to steady flow. However, this is often more realistic according to the reality. [41]

3.1.3 Reynolds number

The Reynolds number, Re , is a dimensionless number that determines the flow regime. The flow regime can be divided into three parts; laminar-, transitional- and turbulent flow where the value of the Reynolds number gives a rough estimate of the friction force in the overall flow. Further, the range of these values for the three parts are stated in table 3.1. [41]

Table 3.1: The range of Reynolds number for the different flow regimes in pipes

Flow regime	Reynolds number
Laminar	$Re \lesssim 2300$
Transitional	$2300 \lesssim Re \lesssim 4000$
Turbulent	$Re \gtrsim 4000$

For laminar flow, the friction factor is independent of the surface roughness and only affected by the Reynolds number. Further, the definition of the Reynolds number given in equation 3.8 is dependent on the average velocity and hydraulic diameter as well as the properties of the air. [41]

$$Re \equiv \frac{\rho V_{avg} D_h}{\mu} \quad (3.8)$$

Transition to turbulence of flow due to obstacles

As previously described in chapter 2, the filament of the spacer contributed as an obstacles that could introduce transition to turbulent flow for larger Reynolds numbers [24, 27, 29, 35]. The occurrence has been described by Bird et al. [43] for fluid flowing around a cylinder, and the various regimes with increasing Reynolds numbers are given in figure 3.1.

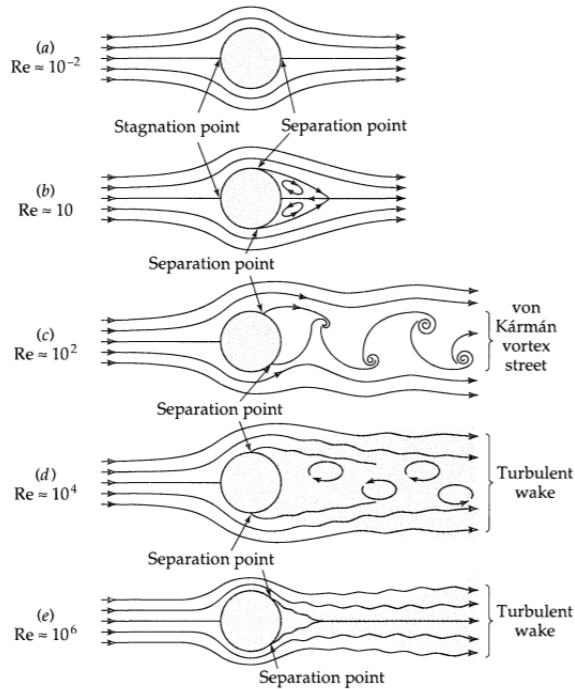


Figure 3.1: Flow behaviors around a cylinder for various regimes as the Reynolds number increases (reprinted with permission [43])

For $Re \ll 1$ shown in (a), the fluctuations of the flow near the cylinder rapidly dies out, giving that the flow is orderly. When the Re reaches about 10, it may be seen in (b) that a pair of vortices occurs behind the cylinder. It has been observed that this type of flow continues up to Re of about 40, when the streamlines separates from the solid surface and creating two “separation points”. Further, when the fluid vortices begin to “peel off” the cylinder and move downstream, the flow has become permanently unsteady. A further increase in Re results in a regularly separation of vortices from alternate sides of the cylinder known as a “von Kármán vortex street”, which is shown in (c). The disorderly fluctuation motion (turbulence) in the wake as seen in (d) occurs with further increase of Re . Turbulence occurs upstream of the separation point for Re about 10^6 and the wake abruptly narrows down as given in (e). [43]

3.1.4 Entrance region in a channel

The entrance region is dependent on when the fluid flow is fully developed for both velocity and temperature profiles. For the profiles to be fully developed, they must remain unchanged and at this point the entry region is said to end. If the profiles for velocity and temperature do not remain unchanged from the same place, they must be differentiated into hydrodynamic or thermal entry length region respectively. [41] However, for the present thesis only hydrodynamic entry length will be considered since the temperature is not being evaluated.

When considering the hydrodynamic entry length, the velocity profile is fully developed when the relation given in the equation 3.9 below is obtained. Further, the formula of the entry length for laminar flow is given in equation 3.10. [41]

$$\frac{\partial(r, x)}{\partial x} = 0 \rightarrow u = u(r) \quad (3.9)$$

$$\frac{L_{h,laminar}}{D_h} \cong 0.05Re \quad (3.10)$$

To assure that the hydraulic entry length is fully developed for a laminar flow, equation 3.10 can be rearranged to state the hydraulic length as given in equation 3.11 for a circular pipe. Although, this is equivalent to other geometries accordingly due to the hydraulic diameter.

$$L_{h,laminar} = 0.05ReD_h \quad (3.11)$$

It can often be assumed that the entrance length is neglectable small compared to the total length of the pipe. If it has to be considered, the developing flow will increase the pressure drop due to the largest obtained wall shear stress. Thus, the effect of the entrance region will increase the average pressure drop for the entire pipe. [41]

3.2 Pressure drop

If a situation requires work to overcome a pressure, it is common to refer to it as pressure drop. [41] This would be the case of an exchanger, but first the pressure will be further explained.

3.2.1 Pressure

Pressure is defined as a “normal force exerted by a fluid per unit area” [41]. Further, the total pressure can be derived from static-, dynamic- and hydrostatic pressure. First, the static pressure is the actual thermodynamic pressure of the fluid. The dynamic pressure is represented by a fluid in motion coming to a stop isotopically. The last term is the hydrostatic pressure, which accounts for the elevation effects such as the weight of fluid on pressure. In a real sense, the term is not pressure since it is dependent on a selected reference level. [41] Further, statical pressure will be of interest in the thesis.

A fluid in motion exerts static pressure on any plane parallel to the direction of motion [44]. Thus, to measure the static pressure, tiny holes are drilled perpendicular to the surface called statical pressure taps or wall taps. When wall taps are created, the measuring device will sense the statical pressure at the wall where there are no components of velocity along the axis of the hole. [45] Given this, it is important that the dimensions of the holes are small enough to avoid distortion which is introduced in the flow field, but not too small so the response time increases. Common sources to measurement errors are eddies developed in the hole cavity, fluid turbulence and fluid stagnation in the holes due to obstacles behind the hole. For the eddies inducing recirculation in the cavity results in a statical pressure higher than the pressure on the surface. [46]

3.2.2 Pressure drop and representable equations

The pressure between two points will contribute to a difference which represents a loss, referred to as pressure drop. The quantity of pressure drop is directly related to the power usage concerning a fan or a pump to obtain a fluid flow. It is therefore relevant to concern the pressure drop in this thesis. Concerning the calculation, the friction forces between the two points in a long straight duct contribute to a larger share of the pressure drop while components can contribute with a minor loss. This is divided into major and minor losses respectively and will be described below. [41]

In addition, a well known and important knowledge of fluid flowing in parallel through a structure, is that the pressure drop in one channel represents the total pressure drop for the whole structure. Thus, if the flow branches out in multiple parallel channels (or pipes) and rejoins, the individual resistance in each channel will not enhance different pressure at the point of branch or junction. [41] Also, the pressure drop calculation is conducted for one channel in the MEE. Correspondingly, when considering the spacers, the pressure drop calculations concern one structure of corrugated pitch due to the parallel flow.

Further, the general formula for pressure drop is stated in equation 3.12 when the pressure loss is dependent on the major and minor losses [41]. Respectively, the relations of pressure drops that will be utilized in this thesis, will be presented in section 4.3.

$$\begin{aligned}\Delta P_{total} &= \Delta P_{major} + \Delta P_{minor} \\ &= \sum_i f_{D,i} \frac{L_i}{D_{h,i}} \frac{\rho V_i^2}{2} + \sum_i K_{L,i} \frac{\rho V_i^2}{2}\end{aligned}\quad (3.12)$$

The equation above is used as the basis to obtain a formula that more specifically represents the case. Shah and Sekulić [42] stated a correlation for the pressure drop when the fluid flow was not fully developed when entering the boundary system. The relation given in equation 3.13 where f_{fd} is the fully developed friction factor and $K_{L,\infty}$ is the incremental pressure drop due to the developing flow. Commonly, the friction factor stated in literary is given for the fully developed flow, where this correlation include the developing flow.

$$\Delta P_{total} = \left[4f_{fd} \frac{L}{D_h} + K_{L,\infty} \right] \frac{G^2}{2g_c \rho} \quad (3.13)$$

Further, when considering the pressure drop through a heat exchanger the minor losses due to the air entering and leaving the effective heat exchanger area will impose an extra pressure drop [42]. However, the exchanger in this thesis does not encounter the reduction/expansion when the air enters/leaves the exchanger and will therefore not be considered in the theoretical pressure drop calculations, but could have been included if a full size exchanger was evaluated.

Major losses

The major pressure losses commonly represent the friction forces in straight pipes and ducts, which then contributes to the largest share of the pressure drop. There are two friction factor correlations that needs to be established. The Darcy friction factor, $f_{D,fd}$, can be obtained by the relation of the Fanning friction factor, f_{fd} , which is stated in equation 3.14. [41] The Darcy friction factor will be used for the further calculations. The friction factors are given with the subscription of fd to state the fully developed flow.

$$f_{D,fd} = 4f_{fd} \quad (3.14)$$

Further, the theoretical friction factors that will be used in the present thesis are stated below. The friction factor for the empty channel is stated in equation 3.15 [41]. According to the geometries of a rectangle and sine curve, the friction factors are stated in equation 3.16 and 3.17 respectively [42]. It should be noted that these friction factors are given for

solid surface and not a mesh screen.

$$f_{D,fd, Channel} = 96.00/Re \quad (3.15)$$

$$f_{D,fd, Rectangle} = 24(1 - 1.3553\alpha^* + 1.9467\alpha^{*2} - 1.7012\alpha^{*3} + 0.9564\alpha^{*4} - 0.2537\alpha^{*5})/Re \quad (3.16)$$

$$f_{D,fd, Sinusoidal} = 9.569(1 + 0.0722\alpha^* + 0.8619\alpha^{*2} - 0.8314\alpha^{*3} + 0.2907\alpha^{*4} - 0.0338\alpha^{*5})/Re \quad (3.17)$$

The description and formula of α^* were given in equation 3.5, whereas the friction factor for the rectangle and sinusoidal geometries are valid for:

$$\text{Rectangle} \quad 0 \leq \alpha^* \leq 1$$

$$\text{Sinusoidal} \quad 0 \leq \alpha^* \leq 2$$

Minor losses

The minor pressure losses are occurring due to typical obstacles in a pipe or duct such as fittings, elbows, contractions and so on [41]. For the case of the MEE, the minor losses are caused by the change of airflow direction through the exchanger and the developing flow.

The different minor losses utilized in the theoretical pressure drop calculations are stated in table 3.2, for the relevant geometries. The minor loss related to developing flow, $K_{L,\infty}$, was directly applied when the values were tabalized in *Fundamentals of heat exchanger design* [42]. However, the values that were stated were given for another α^* for the sinusoidal geometry of $\alpha^* = \sqrt{3}/2$.

Further, the tableted loss coefficient for bends in ventilation ducts from *ASHRAE* [47] had a area ratio that was larger than for this thesis. Thus, the given values for losses due to bends (given in table B.1) was curve fitted so it would be compatible for all aspect ratios. The explanation and equations according to the curve fitting are given in further details in Appendix B.

Table 3.2: Minor losses applied to the pressure drop calculations

	$K_{L,\infty}$ [42]	$K_{L,bend 45^\circ}$
Rectangle	0.674	$-0.045 \times \ln(L_{cross}/H)$
Sinusoidal	1.739	$-0.045 \times \ln(2a_{wave}/h)$

Modelling of spacer geometry and pressure drop

This chapter states the mathematical models that represents the quasi-counter MEE considered in the present thesis. That includes the geometrical shapes of the evaluated spacers, the representative equations regarding the geometries and the formulas needed to calculate the porosities. Further, the pressure drop equation utilized in the thesis is stated along with a friction factor correlation making the experimental pressure drop results comparable to other studies.

4.1 Geometries applied to the spacers inserted into the MEE

For the spacers that were established in this thesis, two geometries were conducted. Regarding the geometry concerning the smallest corrugation pitch achieved a sinusoidal shape, whereas the larger corrugation pitch obtained a geometry that could remind of a ramp. As previously mentioned, other geometries were also evaluated by the author [1] in her previous work. However, some would be hard to create and implement and was therefore eliminated for further investigation.

4.1.1 Ramp spacer

As stated, one of the spacer geometries became more like a rectangle rather than sinusoidal curve. For the pressure drop calculations, these spacers were calculated with the geometry of a rectangle due to available literature. The reason for the different spacers will be

stated in section 5.1.2. Further, the spacer got the geometry as shown in figure 4.1 when considered in flow direction.

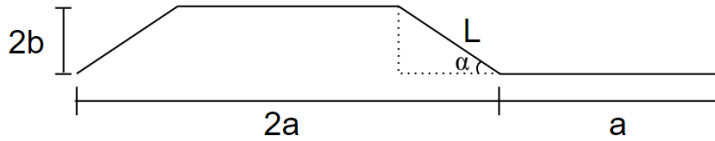


Figure 4.1: Structure of ramp geometry

Since the concerning geometry is considered as a ramp, Pythagoras will be utilized to derive the length of the hypotenuse L_{ramp} . Equation 4.1 states one way to use the trigonometric functions to calculate the angle α , where the formula of tangent is utilized, which must be calculated first.

$$\alpha = \arctan\left(\frac{2b}{a/2}\right) = \arctan\left(\frac{4b}{a}\right) \quad (4.1)$$

Accordingly, the hypotenuse L_{ramp} is then given in equation 4.2. The length will vary with the width of the corrugated pitch and height of the channel, which influences the angle α as given above.

$$L_{ramp} = \frac{2b}{\sin \alpha} \quad (4.2)$$

Further, the number of waves given for the ramp is stated in equation 4.3. The length of one corrugation pitch has been considered as one full cycle which is shown in the figure above. Therefore, the equation is divided by $3a$.

$$n_{waves, ramp} = \frac{W}{3a} \quad (4.3)$$

4.1.2 Sinusoidal spacer

The sinusoidal geometry regarding some of the spacers is shown in figure 4.2. The corrugated pitch and the height have the notations of $2a$ and $2b$ respectively.

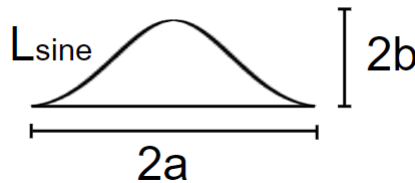


Figure 4.2: Structure of sine curve

Being able to calculate the length of the sinusoidal wave, L_{sine} , the function of a sinusoidal curve can be utilized as given in equation 4.4. The function is characterized by various parameters where A is the amplitude, k is the number of times the function repeats itself, φ represents the phase shift and d is equilibrium line. [48]

$$L_{sine} = f(x) = A \sin(kx + \varphi) + d \quad (4.4)$$

The function repetition k is given by the relation below where P is the corrugation pitch [48].

$$k = \frac{2\pi}{P}$$

The respective formula for the length of the sinusoidal spacer is given in equation 4.5. The equation describes how the curve will vary with different parameters such as the height ($2b$) and corrugation pitch ($2a$) of the wave.

$$L_{sine} = b \sin\left(\frac{\pi}{a}x - \frac{\pi}{2}\right) + b \quad (4.5)$$

In addition, the definition for cross-sectional area is given in equation 4.6 [49]. To be able to calculate the cross-sectional area for one wave, the integral is given by the width of the wave where i is the value at the beginning and j is the amount at the end.

$$A_c \equiv \int_i^j f(x) dx \quad (4.6)$$

The number of waves that the spacers obtained could be found by the width of the channel and the corrugation pitch. The equation used in the calculations are given in equation 4.7.

$$n_{wave} = \frac{W}{2a} \quad (4.7)$$

The amount of air flowing through one wave in the horizontal direction can be described by the total airflow rate divided by number of waves. Additionally, the number of waves must be counted twice to get the wave channels above and below the spacer. The formula for the airflow rate of each wave channel is given in equation 4.8.

$$\dot{V}_{wave} = \frac{\dot{V}}{2n_{wave}} \quad (4.8)$$

4.2 Equations to calculate porosity

To calculate the porosity of a spacer, there are many correlations that must be considered first and will further be stated. The porosity given for a spacer inside a channel is dependent on the volume of void space over the total volume in the channel. Porosity reaches a larger ratio when less material of the spacer is inside the channel. Equation 4.9 is given for

porosity regarding a general geometry. The unoccupied area in the channel is represented by A , whereas B is the channel. [50]

$$\sigma = \frac{V_A}{V_B} = 1 - \frac{V_{spacer}}{V_{channel}} \quad (4.9)$$

The volume of one channel in a quasi-counter exchanger can easily be found by using equation 4.10. Since the two cross flow areas are identical, they have been treated as one rectangle rather than two triangles as shown in figure 4.3, which is utilized in the equation below.

$$V_{B,channel} = W_{counter} \times (L_{counter} + L_{cross}) \times h \quad (4.10)$$

To simplify further notification of lengths and directions in the exchanger, they are divided into horizontal and vertical directions denoted x and y respectively. Figure 4.3 shows where the representative lengths are located in the exchanger (dotted lines). The airflow will follow the pattern of the quasi-counter arrangement (solid line), whereas the shape of the spacers have been calculated according the actual shape obtained in the thesis given in section 5.1.2. The counter- and cross area will be handled separately to ease the calculations while minimizing the chance of errors.

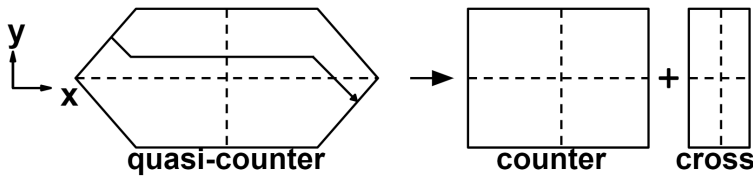


Figure 4.3: Description of the different directions in the exchanger

Further, to calculate the volume of the void space, denoted A in the equation 4.9, the volume of the spacer must first be calculated. Equation 4.11 states the volume for the general spacer i which is dependent on the area of the wire and the total length of the wire for the corrugated screen. The total length of the wire in a spacer can be calculated by equation 4.12.

$$V_{A,spacer i} = A_{spacer i} * L_{total,spacer i} \quad (4.11)$$

$$L_{total,spacer i} = L_{y,spacer i} + L_{x,spacer i} \quad (4.12)$$

Whereas all of the evaluated spacers have circular wires, the common formula for the area is given for a circle in equation 4.13.

$$A_{spacer i} = \pi \times \frac{D^2}{4} \quad (4.13)$$

As stated, before the total length of the wire $L_{total, spacer i}$ can be divided into the horizontal and vertical length. Moreover, different mesh screens, denoted j in these calculations, were experimentally tested in the thesis, obtaining different wire thicknesses and mesh dimensions. The specific values regarding the mesh screens have been stated in section 5.1.2. Thus, to calculate the lengths in x- and y-direction, the length of the mesh $l_{wire, mesh j}$ can be found in table 5.2.

The horizontal length, $L_{x, spacer i}$, is the easiest to calculate when the wire in this direction will be treated as straight lines. Equation 4.14 gives the formula for calculating this length, which is dependent on the length of one wire in x-direction and the amount of wires in y-direction. The amount of vertical wires are dependent on the width of the exchanger and the distance between the wires in the mesh $l_{wire, mesh j}$ in the y-direction.

$$L_{x, spacer i} = L_{exchanger} \times n_{y, wire j} = (L_{counter} + L_{cross}) \times \frac{W_{counter}}{l_{wire, mesh j}} \quad (4.14)$$

The calculation of the vertical length, $L_{y, spacer i}$, is a bit more complicated. The general formula is stated in equation 4.15, whereas the length of one wire, $L_{y, wire i}$, in y-direction is dependent on the geometry of the spacer which are given below. The number of horizontal wires are dependent on the total length of the exchanger and the distance between the wires in the mesh $l_{wire, mesh j}$.

$$L_{y, spacer i} = L_{y, wire j} \times n_{x, wire j} = L_{y, wire j} \times \frac{L_{counter} + L_{cross}}{l_{wire, mesh j}} \quad (4.15)$$

Further, to be able to calculate the vertical length of the spacer, the number of waves must be known. The present thesis will consider different corrugated pitches and the number of waves will therefore vary. However, the number of waves are dependent on the geometry of the spacers and is stated below.

Ramp spacer According to the spacers obtaining a geometry that was more closely related to the rectangular geometry and has been referred to as a ramp. The shape of the ramp was previously shown in figure 4.1.

The length of one vertical wire $L_{y, wire j}$ for the ramp geometry is stated in equation 4.16. In addition, the formula of the length of the hypotenuse L_{ramp} was given in equation 4.2.

$$L_{y, wire j} = 2 \times (L_{ramp} + a) \times n_{waves, ramp} \quad (4.16)$$

Sinusoidal spacer Regarding the spacers obtaining the geometry of a sinusoidal curve, the length of one wire in vertical direction is given in equation 4.17. The length of one curve L_{sine} and the number of waves $n_{waves, sine}$ were stated in equation 4.5 and 4.7 respectively.

$$L_{y, wire j} = 2 \times L_{sine} \times n_{waves, sine} \quad (4.17)$$

4.3 Pressure drop equation utilized in calculations

Pressure drop calculations were conducted for the empty and spacer-filled channels. Regarding the empty channels, the calculations easily conducted. However, when calculating the pressure drop through the ramp and sinusoidal spacer, the surface of the spacers were considered as solid rather than mesh. This was due to the complexity of the calculations for a mesh spacer.

Further, the author conducted a MATLAB-script to calculate the pressure drop in the previous project work during the fall semester [1]. However, the script was not optimally working and has therefore been rewritten to only contain the integral for the sinusoidal cross-sectional area. The rewritten script is given in Appendix C. Accordingly, the main calculations were conducted in a spreadsheet in Excel.

Regarding the pressure drop calculations, the flow has been considered to be following the path of the quasi-counter arrangement, as shown in figure 4.4. Thus, when the airflow has entered the exchanger, the flow has to change direction two times. Respectively, the $K_{L,bend}$ for the quasi-counter exchanger had to be considered twice for both flow directional changes through the exchanger. Additionally, the angle of the air direction change was be 45° both times.

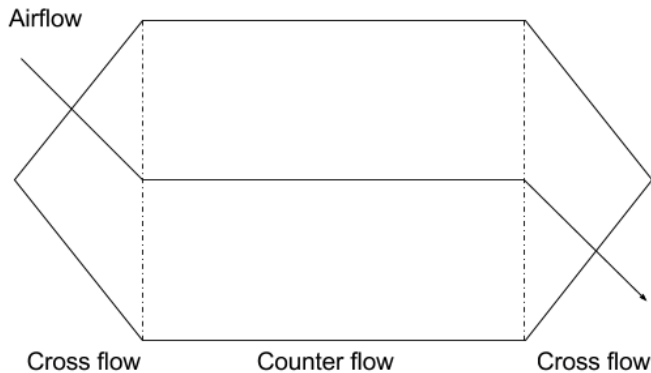


Figure 4.4: Description of the different directions in the exchanger

Accordingly, the total pressure drop for the quasi-counter arrangement will be calculated by the use of equation 4.18, which has been specified for the case in the present thesis. It can be seen that the equation is divided into counter- and cross areas, whereas the cross flow area will be treated as a square (as shown in figure 1.2) and not as a rectangle as it was done for porosity calculation in section 4.2.

$$\Delta P_{total} = \underbrace{\left(f_D \frac{L}{D_h} + K_{L,bend} \right) \frac{\rho V_{avg}^2}{2}}_{\text{counter}} + \underbrace{\left(f_D \frac{L}{D_h} + K_{L,bend} + K_{L,\infty} \right) \frac{\rho V_{avg}^2}{2}}_{\text{cross}} \quad (4.18)$$

4.4 Pressure drop comparison

To compare the results from the experimental testing conducted in this thesis with other studies, either the pressure drop or the friction factor can be utilized. Both comparison methods will be further explained.

4.4.1 Friction factor correlation

Being able to compare the experimental pressure drop results with other studies, the friction factor can be utilized. The friction factor can be found by rearranging the equation for the major pressure drop given in the first term of equation 3.12. When rearranging the general pressure drop equation and eliminating minor losses, the friction factor can be calculated by the use of equation 4.19.

$$f_D = \frac{2D_h \Delta P_{exp}}{L \rho V_{avg}^2} \quad (4.19)$$

The hydraulic diameter can be obtained from the definition of the Reynolds number, given in equation 3.8. Thus, the hydraulic diameter based on the Reynolds number is given in equation 4.20. Importantly, the results are only comparable to other studies if the calculation of the hydraulic diameter was conducted in the same manner.

$$D_h = \frac{\mu Re}{\rho V_{avg}} \quad (4.20)$$

By combining equation 4.19 and 4.20, the friction factor dependent on the Reynolds number is stated in equation 4.21.

$$f_D = \frac{2\mu \Delta P_{exp}}{L \rho^2 V_{avg}^3} \times Re \quad (4.21)$$

4.4.2 Pressure drop correlation to previous study at NTNU

To be able to compare the pressure drop result from this thesis to the results obtained by P. Liu [20], the pressure drop had to be utilized. Even though the exchanger structures were identical, Liu utilized another calculation method of the hydraulic diameter and pressure drop so the results were not directly comparable.

Liu [20] calculated the hydraulic diameter according to the void areas in the channel, excluding the occupied areas of the spacers. The hydraulic diameter was calculated based on the rearranged equation of the Reynolds number stated in equation 4.22 and the use of the maximum velocity.

$$D_h = \frac{\mu Re}{\rho V_{max}} \quad (4.22)$$

The study did not present the pressure drops for the stated airflow rates and representably the Reynolds numbers. Therefore, the pressure drop had to be calculated by using the formula stated in equation 4.23.

$$\Delta P_{exp} = f_D \frac{L}{D_h} \rho \frac{V_{max}^2}{2} \quad (4.23)$$

Further, the present thesis utilizes the averaged velocity to calculate the pressure drop and not the maximum velocity as Liu's research did. Thus, to make the results comparable, the correlation of airflow rate and cross-sectional area had to be applied and is restated in equation 4.24 for the specific case.

$$V_{avg} = \frac{\dot{V}}{\rho A_{c, channel} n_{corrugation pitches}} \quad (4.24)$$

Lastly, the pressure drops according to the largest and lowest friction factor stated in this thesis combined with the calculated average velocities according to the research [20] were calculated so the results could be compared.

Experimental setup and planned experiments

This chapter will state the specific exchanger and the corrugated mesh screens that will be evaluated through experimental testing. Only the pressure drop was measured under isothermal conditions, whereas the heat transfer was neglected. The procedure of assembling the test rig and how the measurements were conducted are also given for the specific case.

5.1 Construction of the quasi-counter MEE

The present thesis concerns a quasi-counter exchanger, where the pressure drop is experimentally evaluated through the channels. The pressure drops through the exchanger are losses due to the exchanger structure, spacers and the membrane. Therefore, optimal solutions should be chosen to minimize the losses. Pressure drop caused by the exchanger, such as friction and losses due to bends are inevitable. However, the pressure drop imposed by the spacer can be minimized by optimal structure that also manage to keep the membrane steady. Thus, the different elements chosen for the exchanger was selected with care and is further described below.

5.1.1 Exchanger structure

In previous work conducted by the author [1], different parameters affecting the pressure drop such as the size of the cross flow area, as well as width, height and length of the channel were mathematically investigated. However, the latent and sensible effectiveness

were also in the necessity of being evaluated along with the pressure to ensure a well performing energy exchanger.

Since the present thesis only concerns the pressure drop through an exchanger and not the efficiencies, the exchanger structure was selected based on previous work done at NTNU. P. Liu [20] constructed an exchanger that achieved good latent and sensible effectiveness in cold climates and the exchanger parameters was therefore chosen for further pressure investigations. From the previous work done by the author [1], the chosen exchanger structure did not impose the lowest pressure drop nor the worst. As stated earlier, parallel channels impose equal pressure drop in all channels and the number of channels can therefore be reduced to one. However, to be able to evaluate the spacers' ability to keep the membrane in place, the rig was designed with two channels representing supply and exhaust air channels.

To investigate the statical pressure at different locations at the inlet and outlet area for both channels, six pressure taps in each channel were created. The pressure drop was found by measuring the pressure difference over the corresponding pressure taps at the inlet and outlet for one channel. The taps were named based on the location over the inlet/outlet areas and at what channel they were located at. Figure 5.1 shows the two channels with corresponding named taps. For the supply channel the taps are named *a*, *b* and *c*, whereas the taps are called *d*, *e* and *f* at the exhaust channel. Further, for the experimental testing, the supply and exhaust channel will vary. Thus, the channel with the O-ring is denoted as *Channel A* and the one without is called *Channel B* to differentiate the channels.

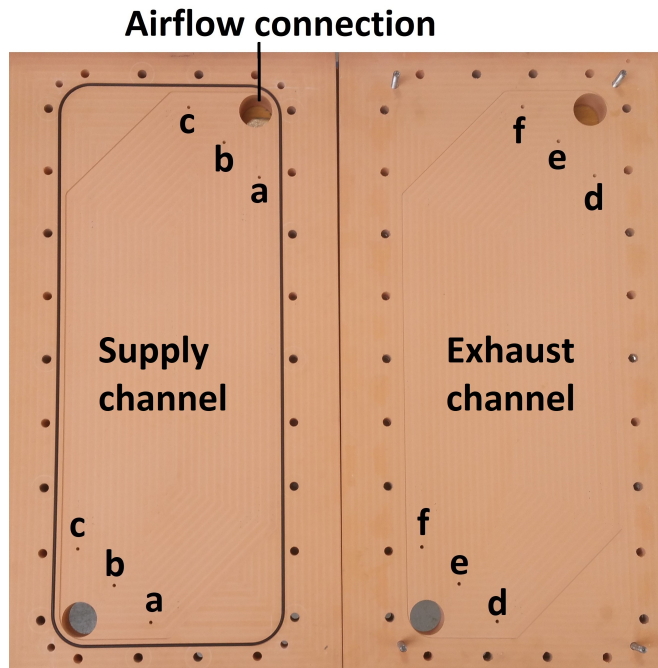


Figure 5.1: The exchanger channels with named pressure taps and channels

Additionally, table 5.1 gives a summary of the values associated with the exchanger casing. Since the CNC milling cutter that carved out the exchanger has high precision, thus the stated dimensions are exactly as what they were drawn to be.

Table 5.1: Specific physical properties for the exchanger casing

Parameters	Value	Reference
Channels pr. flow direction	1	Lab measurement
Half duct height [mm]	1	Lab measurement
Half inlet duct width [mm]	88.4	Lab measurement
Hydraulic diameter, D_h [mm]	397	Lab measurement
Exchanger width [mm]	250	Lab measurement
Exchanger length [mm]	400	Lab measurement
Exchanger height [mm]	2	Lab measurement
Angle cross flow inlet [°]	45	Lab measurement

Inlet- and outlet area

To ensure that the air would evenly distribute into the channels, the inlet area was thoroughly investigated. A test demo was created that illustrate the inlet and where different diffusion materials as well as shapes could be examined. The diffusion material was intended to ensure even air distribution in the channel. The testing included velocity measurements and use of ssvol gas to see the air distribution at the edge of the inlet area. Figure 5.2 shows the test demo (a), the inside of the inlet demo (b) and the investigated diffusion material (c). However, the best result was for an inlet area without diffusion material, which was chosen for the exchanger. Appendix D gives more specifics of the procedure, materials and results for an empty inlet area.

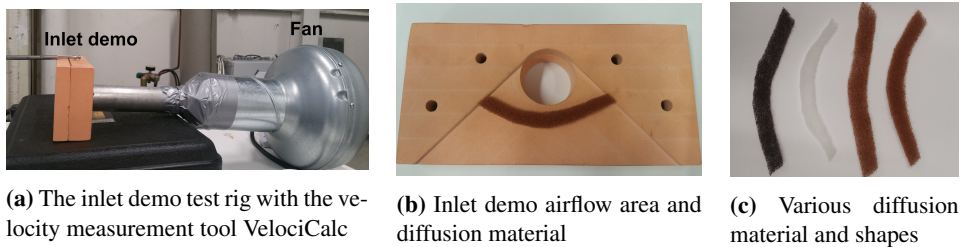


Figure 5.2: The inlet demo and testing procedure

Further, the inlet and outlet area is shown in details in figure 5.3. Concerning the inlet area, the air enters through a duct located perpendicular to the exchanger channel. Due to large duct dimension, the air will keep a low velocity when entering the channel. The air entering the channel reaches an expanding triangle, as shown in figure 5.2b. The system boundary is the effective exchanger area with the shape of the quasi-counter structure,

where the pressure drop is being measured as close the too boundary walls as possibly. For the outlet air, the air will flow in opposite direction.

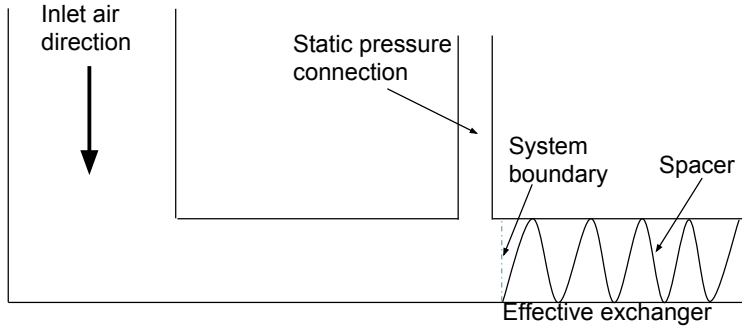


Figure 5.3: Detailed description of the inlet/outlet part

5.1.2 Corrugated mesh screen

Corrugated mesh screen is another name for the spacer that is inserted into all the exchanger channels to obtain the channel height. As previously described, this is to ensure the membrane from fluctuating and deforming the channel geometry. However, how well the spacer is performing to obtain the channel geometry will depend on the geometry of the spacer, frequency of the corrugations of the mesh and the durability to mention some.

Before selecting spacer geometries that would undergo experimental testing, several geometries were mathematical investigated according to pressure drop in a previous work done by the author [1]. The chosen geometry will be stated below. In addition, the general spacer obtaining a structure of the channel arrangement is given in figure 5.4.

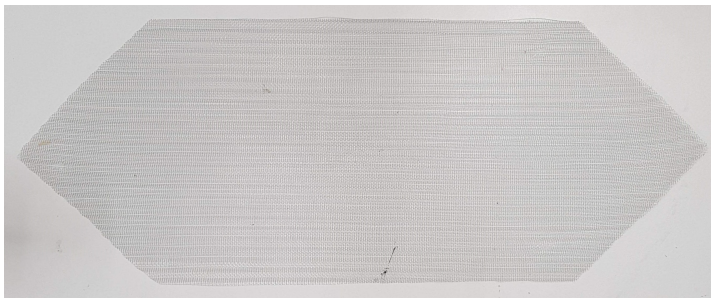


Figure 5.4: The general spacer structure with sinusoidal geometry

Further will the procedure of creating corrugated mesh screens be described. This consist of the chosen metal mesh and the moulds that were created.

Metal mesh

Various dimensions of woven metal screens were investigated in the experiment. When selecting the mesh screens, the wire thickness was wanted to be the same regarding the screens whereas the mesh dimensions varied. This was to be able to evaluate the influence of mesh dimension on the pressure drop. Table 5.2 gives an overview of the different mesh screens and it can be seen that the different screens obtained a similar wire thickness, while the mesh size were varying. All aluminium screens were delivered by *Anping County Bingrong Wire Mesh Products Co.,LTD* [51].

Table 5.2: Specific properties of the meshes

Type	Material	Wire thickness [mm]	Mesh size [mm x mm]
I	Aluminium- Magnesium Alloy	0.2	2.00 x 1.68
II	Aluminium- Magnesium Alloy	0.22	1.41 x 1.41
III	Aluminium- Magnesium Alloy	0.22	1.19 x 1.19

The mesh screens seem to vary some according to the stated dimensions above and the actual fabricated dimensions, whereas the delivered screens were measured for wire thickness and mesh size. However, the measurements were inaccurate due to the small values. It was difficult not to move the meshes or squeeze the measurement tool to hard deforming the screen wire. Thus, the dimensions given in table 5.2 might vary some regarding the actual mesh screen, but how much can not be said for certain.

Mould

The created moulds were used to corrugate the mesh screens into spacers. The ideal experiment would test different moulds obtaining various corrugation pitches, also being referred to as the period, and geometries, where the effect of this would be evaluated by the pressure drop. Thus, for the experimental testing, the chosen corrugation pitches were 10- and 20 mm based on pressure drop calculations, which will further be referred to as Mould 1 and 2 respectively. According to these periods, they were chosen with some deviation so the ability to keep the membrane in place also could be examined.

Formerly, it was intended that the mould spikes would follow the same path as the airflow giving the spacer the shape of the quasi-counter exchanger. However, creating the moulds with the angled area (cross flow) became complex when the corrugated pitch obtained a smaller value than the period of the straight area (counter flow). Also, the screen mesh was not durable enough to ensure the angled pattern when being corrugated due to rupture during all attempts.

Further, the moulds created in this thesis are given in figure 5.5. Both moulds obtained straight lines for the spikes, as shown in figure 5.5a, and the darker lines represent the spacer when the screen is corrugated and cut into the channel shape. Further, the cross-sectional view of the moulds are given in figure 5.5b and 5.5c respectively for Mould 1 and 2 where it can be seen that both moulds had triangular spikes. The belonging notation of the corrugated pitch (P) and height (h) are given for both moulds and the apex angle (β) is given for Mould 1. Specific values regarding the conducted moulds are given in Appendix E.

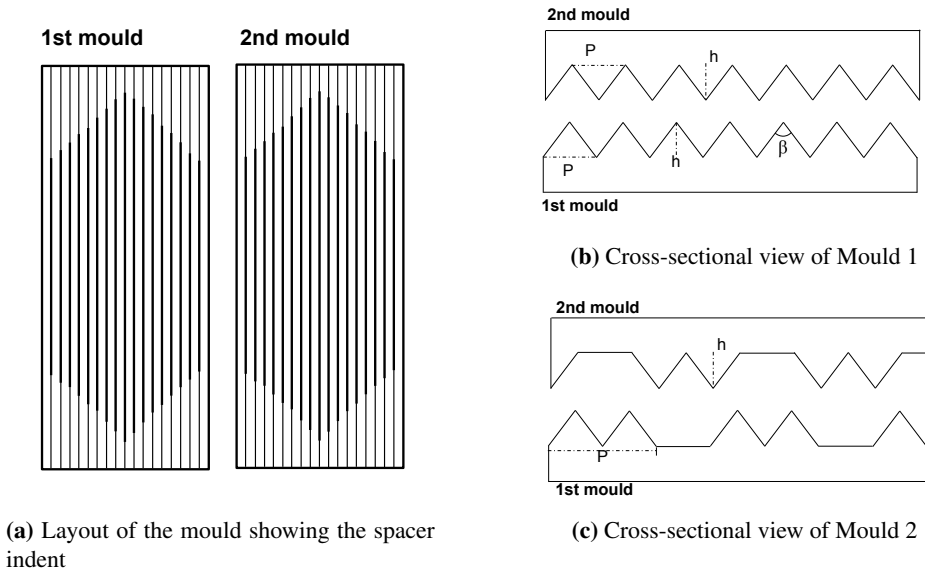


Figure 5.5: The mould imprint and the cross-sectional view of Mould 1 and 2

Mould 2 was created by removing every third spike of Mould 1, doubling the size of the corrugation pitch. To ensure that the mesh screen would corrugate, the mesh would be in contact with the mould wall on both sides when pushed, as figure 5.5c shows. This obtained a spacer geometry of something in between the sinusoidal and rectangular geometry, which has been referred to as a ramp. Another possibility would have been to remove every second spike, enhancing a sinusoidal geometry of the corrugated mesh. However, it was uncertain if the mesh screen would corrugate properly with the use this method. Due to lack of time, only one mould could be created apart for Mould 1. Therefore, the first option was created to ensure that the screen would corrugate.

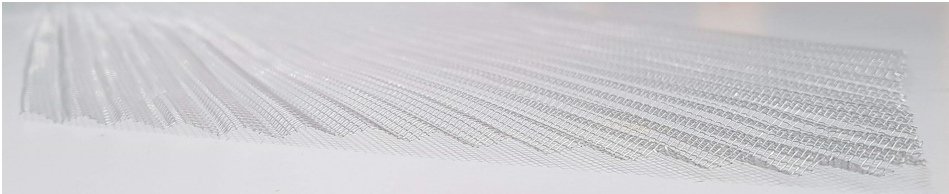
Corrugated spacers

Correspondingly, with the selected mesh screens and moulds the spacers could be created. Since two moulds were constructed, this enhanced respectively two corrugation pitches for the spacers. These spacers have been referred to as Spacer i and ii regarding the lowest and largest pitch which are stated in table 5.3. The corrugation pitches is given as P and apex angle is given as β are described above. As known, the number of waves represents the frequency of the corrugation of the spacers. To corrugate the spacers, the moulds with mesh screen in between were pressed into shape by the use of a hammer.

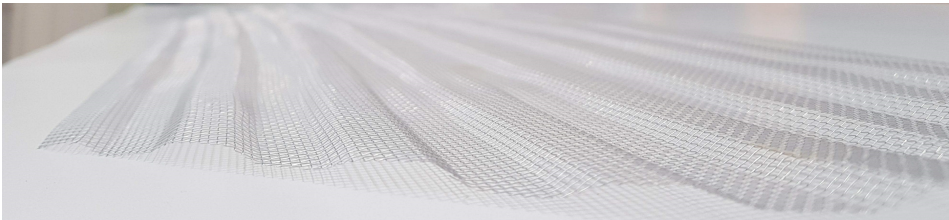
Table 5.3: Specific properties of the corrugated spacers

Spacer	Corrugation pitch [mm]	Height [mm]	Apex angle [°]	Number of waves [-]
i	10	2 + 0.5	136 - 9	25
ii	20	2 + 0.7	-	8.3

As stated, the two different moulds gave different geometries. These geometries are shown in figure 5.6, whereas the spacers with a corrugation pitch of 10 and 20 mm are given in figure 5.6a and 5.6b respectively. The difference in the geometry can clearly be seen, whereas 5.6b obtains a more flat profile. Since the geometry was not sinusoidal, the apex angle was not given in the table above.



(a) Spacer with a corrugated pitch of 10 mm



(b) Spacer with a corrugated pitch of 20 mm

Figure 5.6: Example of the two different periods for the corrugated mesh screens

5.1.3 Membrane

Since the aim of this thesis was to reduce the pressure drop rather than testing the effectiveness of the exchanger, the membrane was substituted by plastic film. The plastic film is from the brand *Caterwrap* which was chosen due to wider film compared to commercial products. The plastic film is not porous and would not diffuse moisture. The properties of the plastic film will closely represent a membrane when it is easy to tear and elastic. Therefore, the representation for the film is assumed to be suitable for this case.

5.2 Experimental Facilities

The test facility is located at the department of Energy and Process engineering at NTNU. The quasi-counter membrane energy exchanger can be used for further pressure drop testing, where other spacers easily can be evaluated.

An experimental facility has been built by the author to evaluate the pressure drop caused by spacer constructions. The test rig has therefore been built in such manner that changing spacers easily can be done. Further, the rig consists of a test unit, one fan and measurement instruments. The pressure drop was measured under isothermal conditions since the efficiencies were not evaluated. Thus, the temperature was not an issue and the facility became less complicated to build. Figure 5.7 presents a schematic of the test rig.

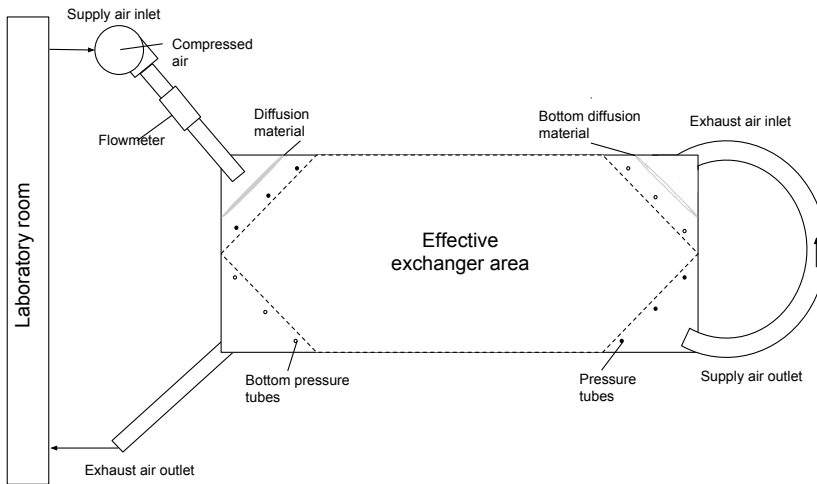


Figure 5.7: Schematic representation of the experimental test rig

As it can be seen from the figure above, the test rig was considered as an open loop. As stated earlier, the effectiveness of the exchanger was not in focus in this thesis. Therefore, the air circulating in the exchanger came from the laboratory room and was not heated nor cooled. Also, since temperature is excluded from the evaluation, the exchanger was not insulated. The air had to be pushed through a flowmeter by compressed air, since a fan was not suitable to supply air when the resistance in the flowmeter was too large. Thus, the rig was therefore connected to compressed air system in the laboratory. The correct amount of air was supplied to the inlet channel by using the control valve of the flowmeter.

To ensure the correct airflow rate in both channels, the air was supplied once into the exchanger whereas the channels were connected by ductwork. It was important that there were no air leakages inside the exchanger, to the outside nor through the duct fittings to ensure the same amount of air in both channels. The air was properly distributed into the channel when entering the inlet area as described earlier. The components utilized to assemble the test rig were airtight, which reduced the risk of any leakages. The ducts used to connect the supply and exhaust channels together, were PP (polypropylene) with appropriate gaskets. Inside the exchanger, a packing (O-ring) was inserted to avoid leakage inside the exchanger. To avoid air leakages to the outside, the two channels were screwed together at multiple locations which sealed the flows inside by the packing. Further, regarding some of the measurements, duct tape was also being utilized at the channel interfaces to ensure airtightness. Different spacers were inserted into the effective exchanger area, where the static pressure drops were measured. When encountering measurements, the test rig was set to stand to ensure no gravity effects on the membrane.

The parameters that were being measured in the present thesis were the airflow rate at the beginning of the loop and the static pressure over the effective energy exchanger area. The airflow was measured and controlled by CT Platon's flowmeter (GTF3AHS). Further, the pressure taps were located at the border of the effective exchanger area. Only the static pressure was assumed to be measured, as stated, when the height difference between the belonging pressure taps were marginal. Thus, the pressure taps were drilled perpendicular to the surface where plastic tubes are connected which was further connected to the measuring device. To evaluate if the pressure drop would vary over the perpendicular line to the cross-sectional area, three pressure taps were drilled into the exchanger as can be seen in figure 5.8 for all inlet and outlet areas. The pressure drop for the different taps were averaged to represent the measured pressure drop. The measuring device that was used, was a micro-manometer from the producer DPM™ (TT570 C).



Figure 5.8: Pressure taps located before the effective exchanger area

5.3 Measurement schedule and execution

According to the experimental testing that were conducted in the present thesis for the different spacers, are given in table 5.4. The mesh and mould parameters are given in further details in table 5.2 and 5.3 respectively. As well as testing the different spacers, an initial test, Test 0, was conducted for the channels with no spacer inside, to establish the pressure drop through the exchanger casing. Test 0 did not incorporate the plastic film either, to be able to evaluate the lowest possible pressure drop. Appendix F summarizes the parameters obtained in each test.

All of the conducted tests were investigated for a varying range of airflow rates to investigate the trends according to the pressure drop. The range of airflow rates were decided based on a wanted range of average velocities inside the channels. Further, the statical pressure drops at all the taps were measured every 15 seconds for one minute for all tested airflow rates. The pressure drop regarding each tap was averaged.

Table 5.4: Summary of which mould and mesh utilized in the different experimental tests

	Mesh I	Mesh II	Mesh III
Wire thickness [mm]	0.2	0.22	0.22
Mesh size [mm x mm]	2.00 x 1.68	1.41 x 1.41	1.19 x 1.19
Mould 1 (P=10 mm)	Test 1	Test 2	Test 3
Mould 2 (P=20 mm)	Test 4	Test 5	Test 6

Due to the stated measurement schedule above, seven different tests were conducted. Regarding the different tests, two assessments were conducted which were denoted I and II. According to the empty channel, these represented different measurements conducted to the channel. As for the spacer-filled channels, the different assessments described the two pairs of spacers conducted for the same test.

Correspondingly, different analyses were conducted for the investigated assessments, whereas the analyses were dependent on the location of where the air was being supplied into the channels. These have been named N (Normal) and T (Turned). Regarding the empty channel, the air was supplied to both ends of Channel B, to investigate if there were any pressure differences between the flow directions through the channel.

According to the spacer-filled channels, channel A and B were both investigated as supply and exhaust channels. When Channel A was conducted as the supply channels it was denoted N and T for Channel B. Thus, the spacers inserted into the various channels could both be evaluated for the effects of being either inside the supply or exhaust channel.

Further, the first pair of spacers (I) were experimentally investigated twice. After the first conducted measurements, the spacers were reinserted into the channels and investigated according to the same procedure as stated above. This was accomplished so the results would minimize constructional errors and uncertainties when the exchanger was reassembled. The pressure drop results were averaged according to the same assessment since it was the same pair of spacers that were investigated.

Lastly, the second pair of spacers (II) were created with the same mesh screens and moulds for the respective tests. This was conducted to ensure that the average pressure drop was durable for more than one set of identical spacers. These tests were conducted in the same manner as described above, but only measured once due to time limit.

5.4 Uncertainty

The uncertainties according to the measured parameters were determined by the method stated in *ENØK i bygninger* [3]. The parameters experimentally evaluated in this thesis is the pressure drop and airflow rate.

Uncertainty can be divided into three main categories; crucial-, systematic- and random errors. Crucial errors are reading errors, misplacing of decimal and so on and it is crucial that it is avoided. Further, systematic error can occur due to hysteresis and friction in the measuring device, using a device that is not calibrated or incorrect execution of measurements to mention some which can be divided into instrumentation- and operator error. The error categories stated above can be avoided. The last category is the random error, which can appear due to unsatisfying measure dynamic and poor resolution of analogue or digital instruments. The errors can not be eliminated, but rather reduced. [3]

To ensure accurate results from experiments, the crucial- and systematic errors should be reduced to a minimum. That is due to these errors not disappearing with repetitively experiments. Thus, when they are eliminated, the repetition of measurements will give numerical values spread around the actual value. The spread is a measure of the random error and interpret how accurate the experimentally measuring was. As stated in chapter 5.2, the measuring instruments are chosen due to easy readability and high resolution.

To calculate the uncertainty of an experimental testing where the results appear directly to the device, known as direct measurements, the corresponding correlation have been utilized. The general uncertainty is stated in equation 5.1. [3]

$$U_r = \pm \sqrt{\frac{s}{\sqrt{n}}} \quad (5.1)$$

$$s = \sqrt{\frac{\sum(x - \bar{x})^2}{n - 1}}$$
$$\bar{x} = \frac{\sum x}{n}$$

However, according to barley excising deviation in the experimental measurement results of the pressure drops, the random error was calculated to be zero.

The flowmeter has been given an accuracy up to ± 1.25 % full scale deflection (FSD) [52]. Regarding the micromanometer, the accuracy of the device was given to be ± 0.05 Pa [53]. The instruments were new when the experimental testing started, which gave accurate calibrations. Thus, the uncertainty according to the instruments have been assumed to be marginal.

Chapter 6

Evaluation of the experimental test rig and conducted testing

The experimental test rig and testing was conducted at NTNU. The author, with help from the laboratory staff and supervisors, design the exchanger and spacers, which was then created. The goal was to construct an exchanger that could easily be opened, easy to be handled and airtight.

The evaluation of the test rig and testing procedure will be given below. With easily accessible laboratory staff and supervisors, correction and measures were easy to implement.

6.1 Evaluation of test rig

The procedure of construction the exchanger casing was extremely accurate due to the precise software and tools regarding the milling machine. The exchanger channels were carved into two separate pieces so the exchanger was opened in the middle. Screws were utilized to keep the exchanger closed. Figure 6.1 shows the setup of the experimental test rig.

When conducting the testing of the different spacers and repetitively, the screw holes got warn. Supplementary, that resulted in some air leakages through the exchanger opening, which introduced errors in the pressure drop measurements. Luckily, the air leakage was detected and new measurements were completed with the use of duct tape to ensure no leakage. The measurement results easily showed when the air leakage had occurred due to much lower pressure drops.

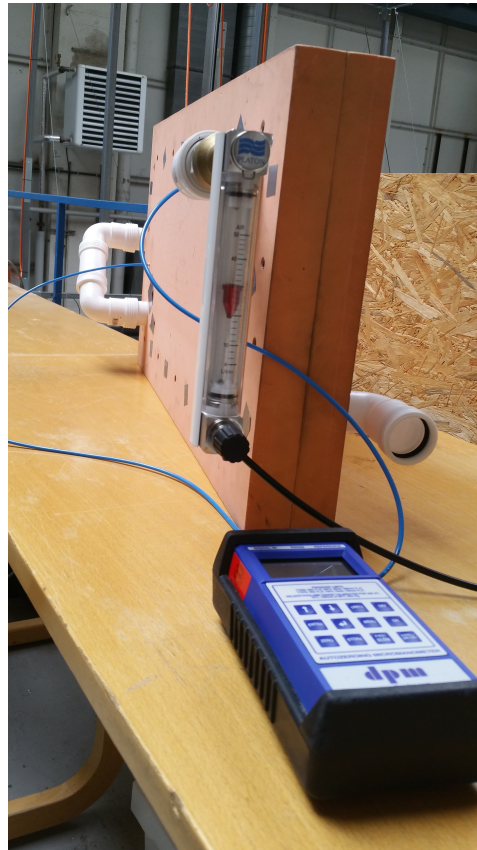


Figure 6.1: The test rig, showing the setup of instruments and pressure tubes.

6.2 Evaluation of the spacers

To create corrugated spacers, mesh screens and moulds were required. The moulds were made of hard plastic, which made it durable and managed the corrugation of the meshes. Due to time limit on the thesis, the second mould with the corrugation pitch of 20 mm was create by removing every third spike of the mould with the pitch of 10 mm. Thus, the mould obtained a geometry that could remind of a ramp. Although the sinusoidal geometry was desirable, the mould was created in such manner to ensure that the screen mesh would corrugate.

Ideally, more than two periods should have been tested to further evaluate the influence on the pressure drop, but due to time limit of the thesis and time-consuming process of creating the moulds that was not conducted.

Three different mesh screens were ordered from a supplier. The screens were ordered with the intention that the mesh dimensions would deviate more from each other. However, since both wire thickness and mesh dimensions were of little difference, the porosity barely varied. For further investigation, screens with more variations should be chosen to better understand the influence of the screen on the pressure drop.

Beneficially, the mesh material was made of aluminium, which is a light material. When large stack of channels is located on top of each other with spacers in between, it is necessary that the weight of the spacer will not be too large so the channel heights will not be obtained.

The method utilized to corrugate the mesh screens, were as stated by using a hammer. This method cannot assure the corrugated height to be the same over the whole spacer, nor that the height is exactly the same as the channel height. However, other methods were tested like using a press for local pressure and larger area press, walls machinery and heavy cylinders to roll over the moulds, but the screen mesh ruptured all times. Therefore, the hammer method was still to be used even if some insecurities of the height will occur. However, the larger corrugation height did not encounter any sources to error, when this only would affect the pressure drop.

Due to the screen easily rupturing, a thicker mesh screen should be considered for further investigation. This would increase the durability of the screen which would make it possible to encounter other corrugation methods that would give a more accurate corrugation height, such as a press.

Another aspect that had to be considered, was that the mesh screen would subtract after being corrugated. Thus, the mould had to be created with larger corrugation heights to be able to obtain the minimum wanted corrugated height of the spacer. This was conducted for the moulds in the present thesis, however, when more accurate corrugation methods could not be utilized, the advantaged was minimized.

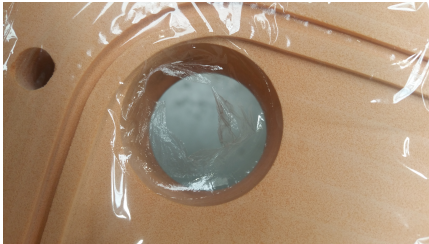
To ensure that the spacers would stay in place when inserted into the channels, they were stapled to the channel walls. The staples were tried to be placed outside the path of the pressure measurement, to avoid an additional pressure drop in the results.

6.3 Evaluation of the testing

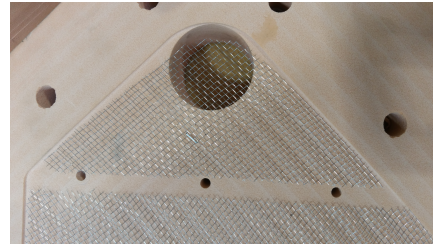
The experimental testing executed in the thesis, were completed in the same manner for all experiments to ensure reliable results. As previously stated, two sets of spacers were made for each test and experimentally tested to ensure reliability in the results. Further, the uncertainty in the pressure drop measurements obtain a value of zero. This was due to the stable results at each pressure tap according to the number of samples during the sample time. However, the pressure drop could have been measured for a longer time period than 1 minute, to ensure that the pressure drop would not vary over time.

After some of the conducted measurements, there were a concern that the results contained static and dynamic pressure due to large holes for the taps. However, the results seemed to give little effect of the dynamical pressure drop when a tube with smaller holes were inserted, where the pressure drop deviated by around 3 % for all airflow rates. This effect would also have contributed to all conducted measurements, where the static pressure drop would have obtained a lower value.

Additionally, when the first tests were conducted, some problems were encountered. The plastic film ruptured over the exhaust channel's outlet, due to being the path with lowest resistance as shown in figure 6.2a. Thus, a measure where some corrugated spacers were shaped as the inlet/outlet area and stapled to the channel wall. This was done to all inlets and outlets to avoid more film ruptures which is shown in figure 6.2b. Further, the measure was located outside the boundary system and was therefore not contributing to the measured pressure drops.



(a) Rupture of plastic film over exhaust outlet



(b) Corrugated mesh to avoid film rupture

Figure 6.2: Plastic film rupture and measures to avoid the occurrence

Theoretical and experimental results

In this chapter, the results for the present thesis are stated. That includes the results from the pressure drop calculations as well as porosity according to the selected spacer. Further, the results from the experimental testing are presented, as well as the pressure drop comparison basis to other studies.

7.1 Results of theoretical calculations

The equations regarding the calculations of porosity for the spacers and the pressure drops have been given in chapter 3 and 4. The calculation was executed for the total pressure drop for the quasi-counter exchanger.

7.1.1 Porosity

The porosity was calculated for the spacers that would be inserted into the exchanger during the experimental testing. The porosity describes the amount of air inside the spacer-filled channel and was calculated according to the equations given in chapter 4.2 for the different geometries. Figure 7.1 gives the results of the calculated porosity according to the experimentally tested spacers and their corrugation pitches. In addition, the tests obtaining the same color have created with the same mesh screen. Further, the different spacers obtained by the testes were stated in section 5.3. Other calculated values according to the porosity have been stated in table G.1 in Appendix G.

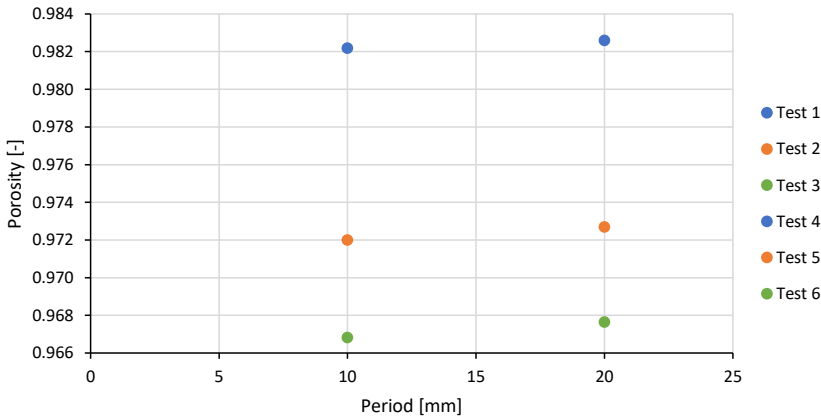


Figure 7.1: The calculated porosity of the conducted experimental tests. Same colors express same mesh screen.

As the figure shows, the tests with the same color varies little in porosity for the different periods. Mesh I (blue) obtained the largest porosity, which was 0.982 and 0.983 regarding the corrugation pitch of 10 and 20 mm respectively, according to having the most porous mesh and smallest wire thickness. The second mesh screen, Mesh II (orange), attained the intermediate value of porosity for both corrugation pitches of 0.972 and 0.973 for the respective periods. Mesh III (green) was the most dense screen investigated in this thesis enhancing the lowest porosity of 0.967 and 0.968. As the result shows, the deviation in porosities are small. Thus, the porosities regarding Mesh III were about 1.5 % smaller for the both periods when compared to Mesh I, with obtains the lowest and largest values. This could indicate that the mesh size and wire thickness of the screen could affect the porosity more than varying the corrugation pitches.

Further, the smallest to largest deviation in the porosity dependent on the mesh for the different corrugation pitches are given by 0.4 and 0.8 ‰ for Mesh I and Mesh III respectively. According to this result, the chosen periods seems to have less affect the porosity as first expected. Due to lack of variation in the dimensions, the porosities encountered a marginal divergence. The values of porosity varied between 0.967-0.983, which gives a deviation of less than 2 %.

7.1.2 Calculated pressure drop

The theoretical calculation of the pressure drop that was performed for the exchanger and the different spacers by using excel as well as MATLAB. The first conducted calculation was for a channel without corrugated screens. The total pressure drop was executed calculated to be 37.3 Pa for the exchanger casing.

Further, the theoretical pressure drop was calculated for different geometries as well as for different corrugated periods. To evaluate the influence of the corrugation pitch on the

pressure drop and being able to choose periods that would be experimentally investigated, different periods were investigated for a constant airflow rate of 30 L/min. The airflow was chosen due to the velocity range that would occur in the channels. Further, the velocity was kept constant whereas the airflow rate through a wave in the spacers would vary according to the change of the periods. The result of the pressure drop due to varying corrugated pitches is presented in figure 7.2. Additionally, other calculated values are given in Appendix H.

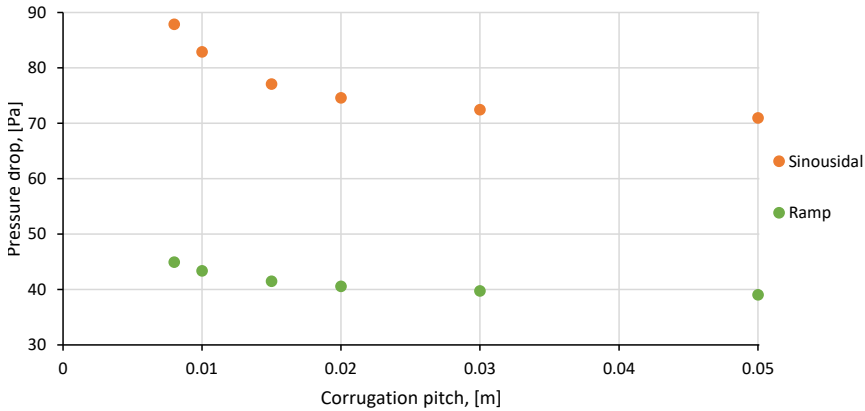


Figure 7.2: Theoretical pressure drop for ramp and sinusoidal geometry of the spacer for an airflow rate of 30 L/min

The figure gives the pressure drop for the ramp (green) and sinusoidal (orange) geometries according to corrugation pitches. It can be seen that the pressure drop for the sinusoidal geometry is decreasing according to the periods, and is starting to stabilize for the period of 0.03 m. According to the ramp geometry, the pressure drop was about halved compared to the sinusoidal geometry for all investigated corrugation pitches. It can also be seen that the pressure drop is getting more stable around the corrugation pitch of 0.02 m.

To achieve the lowest pressure drop, the corrugation pitches chosen for experimental investigation should be as large as possible. However, the spacers must be able to keep the membrane in place and the period could therefore not be chosen at any length. Thus, the corrugation pitches of 10 and 20 mm was chosen for further investigation.

Further, the pressure drop calculations according to the chosen corrugation pitches were conducted for the specific geometries of the spacers where it were dependent on different airflow rates varying within the range of the experimental testing. The result is presented in figure 7.3, whereas the geometries of the spacers are represented by the same icon and the color represents the different corrugation pitches. The result for the empty channel was also included. Other calculated values are stated in Appendix H.

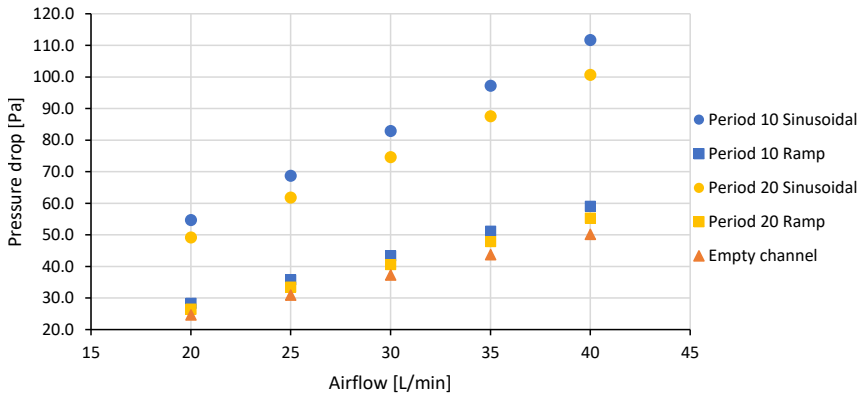


Figure 7.3: Theoretical pressure drop for triangle and sinusoidal geometry of the spacer for the chosen periods

According to the formula of pressure drop, it is known that the pressure drop will increase proportional to the second power of the velocity. Due to the correlation of airflow rate and velocity, the pressure drop is also dependent on the squared of the airflow rate. Thus, with the increase of airflow rate without changing the dimensions of the exchanger, the velocity will increase inside the channel as well as the pressure drop. As the figure shows, the pressure drop is increasing for all calculated geometries, but with different intensity.

According to the two corrugation pitches for sinusoidal spacers, the pressure drop deviation varies between 10.1 and 9.9 % for 20 to 40 L/min respectively. For the case of the ramp geometry, the deviation in pressure drop calculations according to the periods are smaller than for the sinusoidal geometry and was calculated to be 6.5 and 6.3 % for the respective airflow rates. The pressure drop regarding the sinusoidal spacers is approximately the doubled compared to the ramp spacer for all airflow rates. According to the empty channel, the pressure drop is always lower than for the calculations including spacers. The intensity of the change in pressure drop is dependent on the friction factor and minor losses, as well as the hydraulic diameter which varies according to the corrugation pitches and spacer geometries.

The results have been calculated for a solid surface geometry. This would not be the case for the actual spacers that have been experimentally tested. However, due to complicated calculation for a mesh spacer, the solid surface was the only calculation that was undertaken and would therefore only be used as an identification of the pressure drop and to choose the corrugation pitch.

As previously stated, a simplification was conducted whereas the pressure drop has been calculated for the spacer following the same pattern as the flow through the quasi-counter channel. However, this will not be the case for the experimental testing. Yet, it was conducted to incorporate the effect of the directional changes of the flow in the calculations.

7.2 Experimental testing

The experimental test rig and the execution of the different testing were previously explained in section 5.2 and 5.3 respectively. In total, six different spacers were tested varying of mesh screen dimensions and corrugation pitches as well as the empty channel. The pressure drop was measured over multiple pressure taps, but the average pressure drop according to the conducted tests will first be stated to get the general overview of the results. The pressure drop measure in the supply channel obtained a positive value, whereas the exhaust channel obtained a negative value, since the airflows were connected in series. However, all stated values have been given as the absolute value.

The chosen airflow rates in the experimental testing were 20, 30 and 40 L/min which gave the average velocities of 0.67, 1.0 and 1.33 m/s respectively inside the channel.

7.2.1 The average pressure drop results

The average pressure drops through the exchanger and spacers were measured for different airflow rates. Further, the average pressure drop results are given for the empty channel and the different conducted tests in figure 7.4 dependent on the airflow rates. More detailed results of the average pressure drops for the different tests are given in Appendix I.

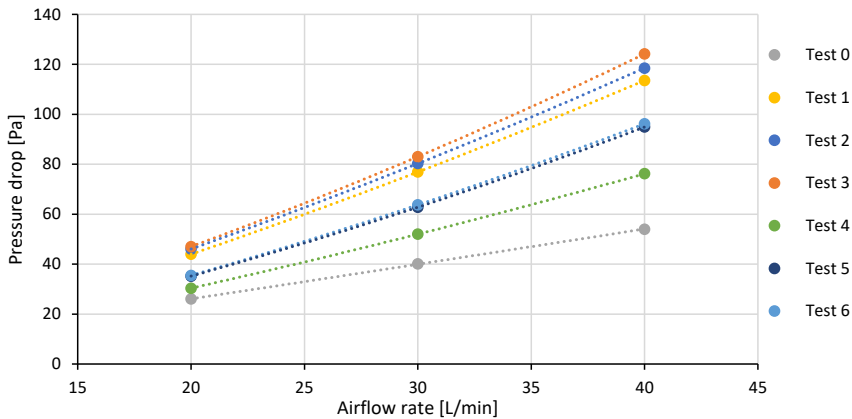


Figure 7.4: The experimental results for the average pressure drop

The figure shows a clear increase in the average pressure drop according to the airflow rate. Also, the increase can seem linearly but as previously known, the pressure is proportional to the squared of the velocity.

Test 0 represents the empty channel, where no spacers were investigated. The membrane, or plastic film, was also left out of the evaluation to achieve the pressure drop that would have been obtained if the exchanger was considered as a flat plate heat exchanger. As

the result shows, the empty channel obtains the lowest pressure drop of the experimental testing, ranging from 26 to 54 Pa with the airflow rates. The deviation between the pressure drops associated to airflow rates increase for the empty channel compared to the tested spacers. The increase in the deviation from Test 0 to Test 4 and Test 3 varied from 14.2 to 29.2 % and 44.6 to 56.5% respectively according to 20 and 40 L/min.

According to the tested spacers, Test 4 achieved the lowest pressure drop through the exchanger for all airflow rates, which varied between 30 and 76 Pa. Respectively, the lowest obtained pressure drop when the average velocity was 1 m/s achieved a value of 52 Pa through the counter flow area. The test was conducted with the most porous spacers, whereas the mesh dimensions were the smallest and the corrugation pitch the largest.

Further, it can be seen that Test 5 and 6 obtain approximately the same pressure drop and are respectively representing the second and third lowest pressure drops. The deviation according to the results of Test 5 and 6 to Test 4 varies from 13.0 to 19.7 % and 14.5 to 20.8 % respectively to the tests and to the increasing airflow rates, which are quite similar for the different tests. In addition, Test 4-6 concern the largest corrugation pitches investigated in the present thesis which obtain the lowest pressure drops.

The largest pressure drop was obtained by Test 3, which concerns the spacers that achieved the lowest porosity. The spacers were conducted by the most dense mesh structure and the lowest corrugation pitch. Respective to the increasing airflow rate, the pressure drops obtain by Test 3 were 47 to 124 Pa. In addition, Test 2 and 1 attained the second and third largest pressure drop respectively. The figure shows a spread in the pressure drop results and Test 1 and 2 are not considerably similar. The deviation in the results according to Test 1 compared with Test 2 and 3 evidently varies by 4.6 to 4.2 % and 6.4 to 8.6 % with the increasing airflow rate.

Furthermore, the figure also shows that the different mesh screens investigated in the present thesis provide a pressure drop from largest to lowest respectively for Mesh III to I for both corrugation pitches. Thus, it is clear that the different mesh screens affect the pressure drop.

In addition, regarding the two corrugation pitches for Mesh I, the pressure drops deviate by 31 to 33 % respectively for the increasing airflow rate. The difference in the deviation is marginal (5.8 %) for the evaluated airflow rates, however, would most likely increase for larger flows. Thus, the larger corrugations seem to be somewhat less vulnerable to the increase of airflow rates, when the pressure drop increase at a slower past than for smaller pitches.

7.2.2 The pressure drop concerning the pressure taps

As previously stated, the investigation for the statical pressure drop were completed at different locations perpendicular to the channel walls. The average pressure drop according to the different tests were stated above. Due to a large amount of data, all the pressure taps measurements are given in tables in Appendix I for the different conducted tests.

The Appendix obtain the pressure drop according to the different taps and the deviation in pressure regarding the different channels, stated as φ . As given in section 5.3, the different assessments conducted for each test, were divided into two which were named I and II. Correspondingly, different analyses were conducted per assessment, which were denoted as N (Normal) and T (Turned). The analyses were dependent on the location of the air being supplied into the channels. Further, the average pressure drop according to the conducted analyses and assessments were also stated in the tables.

It can be seen that for all the conducted tests, the pressure drop regarding the different pressure taps over a channel varies, by more or less. Further, for all measurements, the centre tap obtains the largest pressure drop, whereas the side taps achieve either the same or varying pressure drops which are lower. The occurrence is tried to be explained in section 8.2.2.

According to the channels without spacers, the pressure drops between the pressure taps varied some according to the different analyses. The extensive experimental results can be found in table I.2. At the most, the pressure drop varied by 20 % for 30 L/min according to assessment I and analysis N which obtained the pressure drop of 36 and 45 Pa respectively for the pressure taps a and b. Further, the pressure taps a and c obtained varying results regarding the respective analyses.

In addition, the same analysis as stated above, pressure taps a and c respectively obtained the values of 36 and 43 Pa, which then deviates by 16 %. For the second analysis conducted for the same assessment, the pressure drops regarding the respective pressure taps were not close in values. Yet, the average pressure drops for both analyses obtain the same value. Between the different analyses conducted for the empty channel, the results deviated by most of 3 % for the same airflow rate regarding assessment II.

A general observation regarding the results showed that the pressure drop between the channels regarding the same assessment could vary a lot. However, according to the analyses N and T, the average pressure drop for both analyses obtained the approximate same value. An example of this has been given in table I.7 for Test 5 regarding assessment I and the airflow rate of 40 L/min. According to analysis T, the deviation in pressure drop according to the supply and exhaust channels varied by 46 Pa. Further, for analysis N, the pressure drops between the channels varied by -9 Pa. Yet, the average pressure drops became 46 and -9 Pa for the analyses N and T respectively, which obtained the difference of 2 %. It should be mentioned that these deviations were approximately the same according to all airflow rates. Other examples of this can also be obtained from other tables in Appendix I. It seems like the pair of spacers would contribute to the same pressure drop even though the pressure drop varied over the two spacers.

Some measurements obtained a somewhat similar deviation between the channels for both analysis regarding to the same assessment, but with different signs. This was seen for Test 1 in table I.3 whereas the deviations obtaining for the airflow of 30 L/min were 54 and -46 respective to N and T, for assessment I. Yet, the average pressure drops according to the analyses were 74 Pa for both cases. Further, another case occurring to the results, were that the analyses for the same assessment obtain the same sign. Assessment I in Test 4 obtained this, which is given in table I.6, where the deviations for the airflow of 30 L/min were 13 and 12 and the average pressure drops 48 and 51 Pa respective to analyses N and T. In addition, the average pressure drop was very stable according to the two analyses.

Commonly, the average pressure drops regarding the same assessment obtain often similar values. However, when concerning the different sets of spacers conducted for the same test, the average pressure drop more frequently differed. According to Test 3, with the results stated in table I.5, it can be seen that the average pressure drops according to the assessments, $\Delta \bar{P}_i$, achieved the values of 90 and 76 Pa for the airflow rate of 30 L/min. The discrepancy was calculated to be about 15.5 % according to the airflow rate and vary between 15 and 16 % for the 20 and 40 L/min respectively.

7.3 Pressure drop according this and other studies

To be able to evaluate the pressure drop results from the experimental testing against other studies, either the pressure drop or the friction factor can be utilized. The pressure drop can be directly applied if the dimensions of the exchangers are the same, whereas the friction factor can be used for cases that do not have relative dimensions. As described in section 4.4.1, the friction factor can be derived when the pressure drop through the exchanger is known. The friction factor was calculated to be dependent on the Reynolds number, making the factor comparable to other studies and exchangers.

7.3.1 Friction factor regarding experimental testing

The friction factors from the experimental testing were obtained from power regression of the pressure drop in Excel and figure 7.5 shows the result. For this case, the friction factor correlation is valid for the Reynolds numbers between 174 and 348 respectively given for the airflow rates of 20 and 40 L/min.

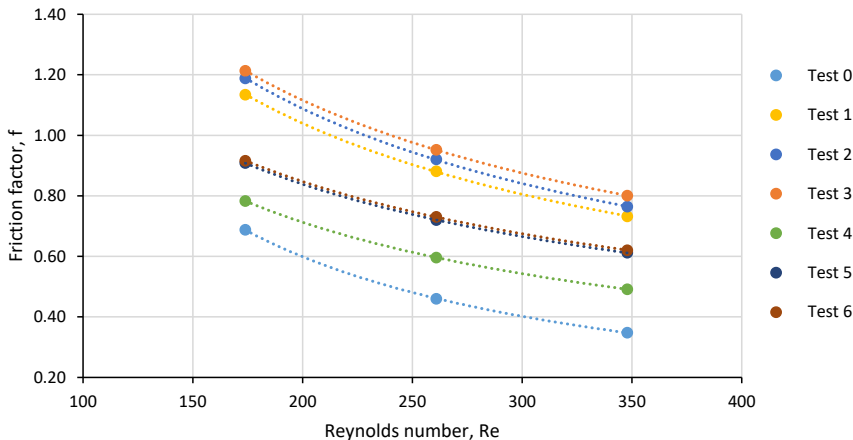


Figure 7.5: The friction factor dependent on the Reynolds number

The friction factor and the coefficient of determination according to the experimental tests are given in equation 7.1.

$$\begin{aligned}
 f_{\text{Test } 0} &= 110.0 \times Re^{-0.98} & R^2 &= 0.99 \\
 f_{\text{Test } 1} &= 29.34 \times Re^{-0.63} & R^2 &= 0.99 \\
 f_{\text{Test } 2} &= 31.70 \times Re^{-0.64} & R^2 &= 1 \\
 f_{\text{Test } 3} &= 26.65 \times Re^{-0.60} & R^2 &= 1 \\
 f_{\text{Test } 4} &= 23.31 \times Re^{-0.67} & R^2 &= 0.99 \\
 f_{\text{Test } 5} &= 17.18 \times Re^{-0.57} & R^2 &= 1 \\
 f_{\text{Test } 6} &= 16.63 \times Re^{-0.56} & R^2 &= 0.99
 \end{aligned} \tag{7.1}$$

In the figure above, the results for the different tests obtain the same patten as for the pressure drop results. This gives that the friction factor correlation is the smallest for the empty channel. Further, Test 4 obtains the lowest friction factor for the evaluated spacers, whereas Test 3 attains the largest.

Additionally, it can be seen from figure 7.5 as well as the formulas in equation 7.1 that Test 1-3 obtained approximately the same friction distribution when the power is about the same, but the equations have different constants. The spacers introduce the same friction factor development and would therefore not intersect if the powers are similar enough. Further, the friction factor correlations for Test 5 and 6 are approximately equivalent due to the similar power and constants in the representative equations, which was also the case for similar pressure drops.

7.3.2 Pressure drop correlation to other studies

As presented earlier, the experimental test rig in the thesis obtained the same dimensions as a previous conducted study at NTNU [40]. The exchanger casings were identical, whereas some modifications were made to the rig in this thesis due to only concerning the pressure drop.

The comparison of the results was more complicated than anticipated, when P. Liu had utilized other correlations for hydraulic diameter, Reynolds number and pressure drop. Thus, the procedure of calculation to compare the pressure drop results was given in section 4.4.2. The pressure drops regarding the values stated in P. Liu's study are given in table 7.1.

Table 7.1: Calculating the pressure drop according to stated values in the study conducted by P. Liu [40]

\dot{V} [L/s]	V_{\max} [m/s]	V_{avg} [m/s]	Re [-]	f [-]	D_h [m]	ΔP [Pa]
4.2	2.0	0.93	387.9	0.428	0.00277	222.1
5.9	2.8	1.31	542.2	0.368	0.00276	375.0
6.9	3.4	1.53	647.2	0.340	0.00272	519.5

For the average airflow rate of 1.31 m/s (5.9 L/s) was calculated to be 375 Pa. In addition, the calculations seemed accurate when the study stated that the pressure drop according to the airflow rate of 7.0 L/s gave 524 Pa. The calculated pressure drop became 519.5 Pa for an airflow rate of 6.9 L/s, which is similar when considering some difference in the airflow rate.

Another observation regarding the results given in the table above, is that the hydraulic diameter varies with the airflow rates. The values should have been the same, but the differences have probably occurred due to lacking decimals in the calculations.

Further, the pressure drops according to the friction factors obtained in this thesis have to be calculated for the average velocities utilized in Liu's study. The correlations of friction factors can be obtained in equation 7.1 where Test 3 and 4 were selected for comparison due to the largest and lowest obtained pressure drop respectively.

The pressure drop regarding the spacers conducted in the present thesis regarding the average velocities utilized in Liu's study are given in table 7.2. The pressure drops regarding the average velocity of 1.31 m/s became 121 and 74 Pa respective to Test 3 and 4.

Table 7.2: The pressure drop according to Test 4 comparable to the study conducted by P. Liu [40]

V_{avg} [m/s]	$\Delta P_{\text{Test 3}}$ [Pa]	$\Delta P_{\text{Test 4}}$ [Pa]
0.93	75.3	47.2
1.31	121.2	74.1
1.53	150.9	91.3

7.3.3 Friction factor according to other studies

Another study has provided its friction factor correlation according to the tested corrugations screens for others to compare with. The study conducted by Woods and Kozubal [24] studied different types of spacers that will be compared to the results obtained in this thesis. Their study gave the experimentally tested friction factors for the mesh spacers within the same range of the Reynolds number as the present thesis and based the hydraulic diameter of the empty channel. The plain-fin triangular spacer was not further relevant for comparison for this thesis and was therefore left out. Thus, figure 7.6 shows a graph for the corrugated mesh screens from Woods and Kozubal's [24] study based on the Re from this thesis.

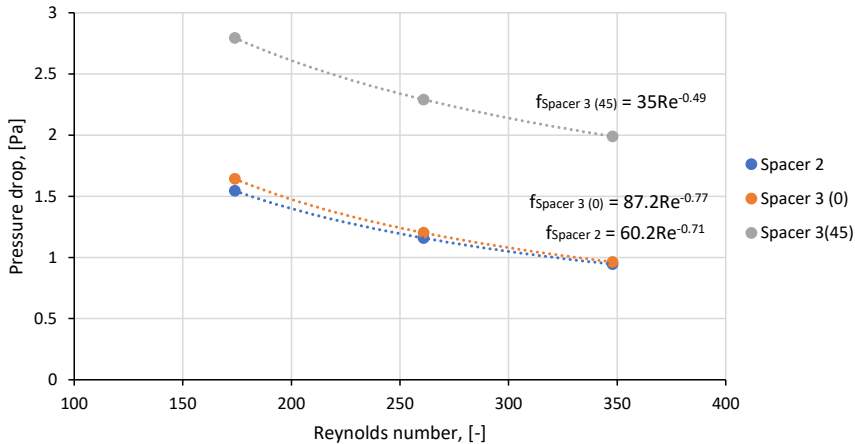


Figure 7.6: Friction factor comparison to Woods and Kozubal's [24] research

The figure shows that the friction factor for the experimentally tested spacers by Woods and Kozubal [24] varied between 2.79 to 0.94 for the largest to lowest value respectively for the Reynolds numbers of 174 to 348. It can be seen that the two different types of spacers enhancing the same flow pattern through the spacers (0 °) obtain approximately similar friction factor distributions. Further, it can also be seen that the attack angle for the airflow greatly influence the friction factor in this case.

Comparison and discussion of results

This chapter gives the comparison and discussion of the previous stated results in chapter 7. First, the theoretical pressure drop calculation will be investigated. Thereby, the comparison and discussion of the experimental results along with the porosity will be stated. The comparison of the experimental results and other studies will be further conducted.

8.1 Investigation of theoretical and experimental pressure drop

The present thesis undertook a theoretical and experimental investigation for the pressure drop for the specific exchanger arrangement and corrugated spacers. The result from both investigations are given in section 7.1.2 and 7.2.1 respectively. The theoretical calculations were foremost conducted due to the selection of corrugation pitch and obtain a theoretical pressure drop according to the exchanger casing. Further, the calculations were obtained to get a better understanding of how the chosen spacers would influence the pressure drop with the increase in airflow rates.

Considering the channel without spacers, results regarding the theoretical and experimental investigations obtained a deviation in the pressure drops of approximately 7 % for all airflow rates. The pressure drop regarding the experimental results obtained a larger value compared to the calculated drop, which would give a larger experimental than theoretical friction factor. According to Woods and Kozubal [24], they also obtain a larger experimental friction factor deviation from the laminar theory, but with the increase of the Reynolds number. They assumed the deviation was encountered by irregularities when the Re got

more dependent on the surface roughness. However, the flow in this case were laminar, so this is not as likely for the particular case.

This deviation could be caused by the flow not being fully developed before entering the boundary system. As previously stated, the occurrence would increase the pressure drop through the exchanger [41]. This effect was being incorporated into the theoretical calculations, however the value for the incremental pressure drop coefficient might not have to be accurate for the specific case when it was a tabulated value. Concerning the experimental investigation, it was conducted without the use of plastic film so this would not encourage a larger pressure drop.

Regarding the spacers, the corrugation pitches were chosen due to the calculations whereas the lowest pitch was chosen for the rapidly reducing pressure drop and the larger pitch when the pressure drop started to stabilize. Also, the decision was based on the concern that the spacers would still have the ability to keep the membrane steady. Further, the pressure drop influenced by the increase of airflow rates for the concerning spacer geometries and corrugation pitches were conducted. However, these results were chosen not to be directly compared to the experimental results due to lack of similarities.

As known, the calculation was conducted for corrugated screens of solid material and not a mesh. Another difference that was not included into the calculations were the deflection and movements of the membrane which would occur during the experiments. Also, the calculations conducted for the ramp geometry were executed for a rectangle when this was the available literature. Thus, to obtain an accurate calculation of the real case, a computer simulation should rather have been used.

Another aspect was the complexity of the pressure drop calculations for mesh spacers, where the wire dimension and mesh size of the screen could not be included in the calculation. This would lead to some inaccuracies because of reduced cross-sectional area and would affect the velocity. Thus, only basing the pressure drop according to the spacers on theoretical calculations, especially for solid surface, could result in large deviations from actual pressure drop.

8.2 Comparison and discussion of the experimental testing

As known, the present thesis created six various spacers according to two different moulds and three mesh screens, that were experimentally investigated. The moulds obtained two different geometries which influenced the corrugated screens shape. The spacers with the corrugation pitch of 10 mm obtained the geometry of sinusoidal waves and the ones of 20 mm achieved the geometry closer to a rectangle, or a ramp as it has been referred to in the thesis.

8.2.1 Different conducted tests

The empty channel achieved the lowest pressure drop according to the experimental testing. Consequently, the result corresponds well with previous stated literature and somewhat the theoretical calculations as stated above. Since corrugated mesh screens were absent from the channels, the airflow was encountering less obstacles inside the channels which would result in less resistance. Respectively, that would introduce a lower friction factor, and the pressure drop was therefore shown to increase at a slower past compared to the tested spacers. Thus, the results showed that the deviation in the pressure drop for the empty channel and Test 4 was increasing with the airflow rate. Further, the same result was obtained for the deviation between the empty channel and Test 3, only at a more significant difference.

Continuously, the tested spacers differed in corrugation pitch and mesh screen dimensions. As known, two set of spacers were created for each test to ensure reliability in the pressure drop results. Figure 8.1 shows a comparison of the calculated porosity and the experimentally measured pressure drop for 30 L/min that was obtain for the respective tests, and will be used as a basis for further comparison of the tested spacers.

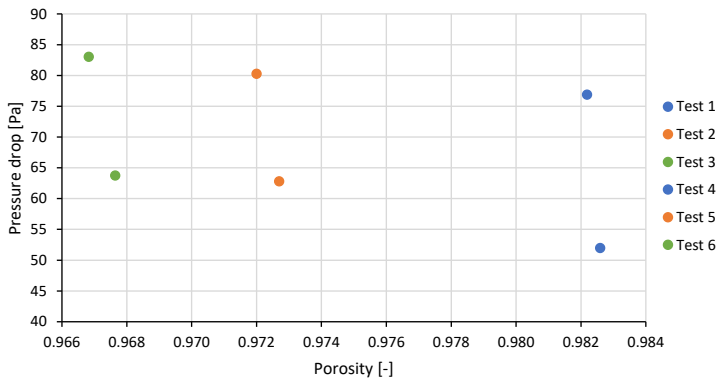


Figure 8.1: The calculated porosity and experimtnal pressure drop respective to the tested spacers for 30 L/min. Same colors express same mesh screen.

Regarding the experimentally tested spacers, the results agreed well with the previous stated literature and theoretical calculations for the different corrugation pitches that were evaluated. The spacers obtaining a larger corrugation pitch achieved lower pressure drops, and opposite, as can be seen in figure 8.1 for Test 4-6. Further, when selecting the corrugation pitches, the value would preferably be as large as possible when concerning the pressure drop. However, the essence of spacers was to keep the membrane from deflecting. Thus, the corrugation pitches could not have been selected to be any particular value. At what value the limit of ability to keep the membrane steady would need further investigation.

Accordingly, the corrugation pitches were selected based on the knowledge that it would influence the porosity. With the increase in porosity, the filament resistance inside the channel would reduce [37]. However, regarding the porosities shown in figure 8.1, the corrugation pitch seemed to have marginal effects on the porosity when it deviated by approximately 1.5 % for both corrugation pitches. Further, it could be stated that the pressure drop was greatly influenced by the corrugation pitch, but also porosity. The porosity enhances a pressure drop deviation of 7 and 18 % respective to the pitch of 10 and 20 mm at 30 L/min. Given this, the porosity affects the pressure drop more greatly for larger corrugation pitches. Thus, the influence of the corrugation pitch on the porosity and hence the pressure drop would need further investigation.

Another important aspect of the different evaluated corrugation pitches, are the different geometries that were obtained. The spacers with a corrugated pitch of 20 mm obtained a rather rectangular shape instead of sinusoidal geometry as was the case of the period of 10 mm. The rectangular shape might help keeping the membrane in place due to two spacers maintaining flat areas where the spacer is placed in between. Yet, the sinusoidal geometry has been proven to be sufficient to keep the membrane from deflection in previous studies [24]. The lower pressure drop results according to the larger corrugation pitch, is most likely coherent to the pitch size, but could also have been influenced by the spacer geometry. So, to ascertain the beneficial effect of the rectangular shape, both geometries have to be evaluated for the same corrugation pitches as well as for a broader spectre of pitches.

Continuously, the mesh screens chosen to be experimentally investigated were named from I to III respectively for the largest to lowest mesh screen dimensions. Initially, it was wanted to evaluate the influence of the mesh dimension on the pressure drop rather than wire thickness. Thus, the dimensions of the wire thicknesses were intended to obtain the same value. However, the screen chosen in this thesis attained some variations according to the thickness and the mesh dimensions did not affect the porosity and pressure drop alone. According to figure 8.1, the respective mesh screens have obtained the same color regarding the different corrugation pitches.

Further, the mesh sizes, especially Mesh II and III, obtained quite similar dimensions. To properly evaluate the influence of porosity, the variation could have been larger. Yet, due to complications to obtain mesh screens with dimensions utilized in the present thesis, contacted suppliers could not deliver more porous meshes. Regarding the calculated porosities, the values might be lower due to lack of double wires at the crossings in the woven mesh. Although, this is assumed not to affect the deviation in porosities according to the tests. A more extensive investigation according to the porosity affecting the pressure drop needs to be conducted when the variation in porosities are larger and more precise calculations are obtained. It could also be evaluated what happens with the pressure drop when the flow passes through the mesh screen for varying mesh dimensions rather than following the corrugated path.

Regarding the evaluated mesh screens, Mesh III was rather stiff. The mesh screen was easier to form and ensure structure when it did not retreat as easily and was more durable after being corrugated. Even though the screen provided the largest pressure drop, the stiffness in a spacer could be beneficial when utilized in an energy exchanger. Thus, the stiff spacer could have encouraged to less deflection inside the exchanger and would thereby ensure durability over time. This might be ensured by a thicker but more porous mesh screen, which would need further investigation.

Initially, the spacers were wanted to be conducted with an angled area at the cross flows, to obtain the same pattern as the flow, which has been stated earlier. As recorded in the literature, the pressure drop can vary a lot due to the attack angle of the airflow facing the spacers [24]. Expectantly, the less resistance the spacers would enhance on the airflow, the smaller the pressure drop would become. Yet, as previously stated, due to complicated creation of the mould and easily rupturable mesh screens, this was not executed for this thesis.

As previously stated, during the experimental testing, air leakages were detected. Fortunately, it was discovered and the results showed when the leakages had occurred. Thus, Test 2-4 and 6 were conducted again, whereas Test 1 and 5 seem to have appropriate results. Regarding the average pressure drop result stated in section 7.2.1, Test 5 and 6 obtain vary similar results whereas Test 2 and 3 had a larger deviation. If both Tests, 2 and 5, had been conducted again, the deviation between in the average pressure drops could have obtained the same pattern. Yet, to ensure durability and stable pressure drop results, all of the tested spacers should be experimentally tested multiple times. This could also vary the obtain pressure drop pattern for the results.

8.2.2 Pressure taps

As known, the measurements were conducted by measuring the pressure drop at different pressure tap locations and where the general observation of the results were given in section 7.2.2, due to a large amount of data.

As the results showed for all tests, the pressure drop varied between the pressure taps belonging to the same channel, whereas the middle tap enhanced the largest pressure drops compared to the side taps for all measurements. However, as stated in the theory, the pressure at the branch or junction is the same value [41]. If the effective exchanger area can be assumed to be a resistance, the air will be divided into “channels” when flowing through the effective area. Thus, some of the air will be diverted out to the sides and some closer to the centerline of the airflow path. However, the pressure drop for all paths are, in literature, the same and should therefore not have been deviated from the between the taps.

One reason could be due to the spacers located at the boarder of system boundary of the pressure measurements which influenced which enhanced deviation. The spacers could initiate vortices with would be detected by pressure measurement, leading to different results. The airflow could have followed the path will the least directional changes, which would be straight through the effective exchanger area. Yet, this path would contain most resistance regarding the spacer mesh. This could initiate a lower velocity, compare the airflows following the path of the corrugated spacers, which would increase the statical pressure for the middle tap. Thus, as known, the total pressure is the sum of static, dynamic and hydrostatic pressure [41]. When hydrostatic pressure is neglected and the velocity is lower which introduce a lower dynamic pressure, the static pressure would become larger to maintain to total pressure.

Another reason could be to irregularities around the pressure taps, enhancing lower or larger statical pressures. The taps were investigated for both channels, yet nothing could be detected. The same tube and measurement device was also utilized, so these should not impose a difference regarding the deviations. Further, the corrugated spacers introduced in the inlet and outlet areas could also have influenced the flow. However, the middle pressure tap obtains larger value regarding the empty channel where no spacers were inserted. Another assumption is that the film would deflect more over the middle area which imposed a larger pressure drop but could not be validated. Hence, the reason for the different pressure drops according to the pressure taps is outside the scope of this thesis and must be further evaluated. A CFD simulation could be conducted to achieve better understanding of why the deviations occur and would further make the pressure drop results according to the spacers more reliable.

Concerning the variations obtained by the different pressure taps for the empty channel, the results were assumed to be more similar than some of the achieved measurements due to no interference of spacers inside the channel. Another reason than the once previously stated for the deviation regarding the taps, could be assumed to occur due to small obstacles or irregularities on the exchanger walls enhancing different pressure drops. The channel height is only 2 mm, so the irregularities do not have to be large to appoint a difference. Yet, why the pressure drops obtained for the different analyses regarding the same assessment is unsure. For both analyses, the exchanger was not opened, so the situation inside the channel should have been the same for both measurements. However, the average pressure drop according to the different analyses are identical or approximately the same. Thus, the occurrence inside the channel does not seem to have a great effect on the overall pressure drop.

The same observation attained for the empty channel occurred for the spacer-filled channels. The variation in pressure drop according to the taps appointed the same channels were assumed to be obtained due to the resistance endured by the spacer filaments. Thus, the pressure drop regarding the appropriate taps could be low due to fortunate placement of spacers and taps, as mentioned above.

Further, if the deviation is larger for only one of the analyses which was positive, that spacer contributed to a larger pressure drop when being used in the exhaust channel, which was given for Test 5 in section 7.2.2. This might be explained by the lack of corrugated height for that spacer or tension in the spacer located in the supply channel, resulting in reduced channel height which increased the pressure drop. Accordingly, that particular spacer might not be as eligible to keep the membrane steady and to obtain channel height. However, another reason for the deviation, could be occurring due to the supply channel being of positive pressure, which then deflect the membrane into the exhaust channel, resulting in larger pressure drop for the negative pressure flow channel. This occurrence has been observed in a previous study, when the membrane was not pre-stressed [25]. It should be mentioned that this only occurred for deviation with large positive values. However, this would need a more extensive research.

In addition, the deviation in the pressure drop between the two channels obtained different range of variation, as stated for Test 1. If the deviation obtains somewhat the same values but with different signs, it was the same spacer contributing to the largest pressure drop. Regarding this case, the pressure drop seems to be mainly affected by the spacer filament and not the movement of membrane, due to both supply and exhaust channels contributing with the largest pressure drop regarding to the respective analyses.

In addition, for some of the measurements, the deviation between the supply and exhaust channels became positive for both analyses regarding the same assessment, which was shown in Test 4. The pressure drops are always largest for the exhaust channel. An interpretation could be that the spacers obtain a similar structure which enhanced the same ability to keep the membrane from deflection.

Regarding the different assessments conducted for each test, two set of identical spacers were created to ensure reliability in the measured results. Further, the obtained results showed that the average pressure drops varied between the assessments, which was stated for Test 3 in the results. This could be due to some deviations in the created spacers whereas they could gain different heights and the cut spacer shape. If the spacers were not perfectly fit into the exchanger casing, there could be some gaps between the exchanger wall and outer spacer edge. However, if the spacers obtain a shape a little larger than the casing, the spacer would retrieve some tension to fit into the channel and deflect. The last incident has been assumed to have to largest contribution to the pressure drop due to deforming the other channel height.

The spacers that were created for this thesis obtained a corrugation height of 2 mm or a little bit larger. Desirably, the height should have obtained a close value to 2 mm to ensure no change in the channel height. Regardless, when the corrugation height of the spacer obtaining at least the channel height, the membrane will have less space to deflect on. This could have enhanced a better performance of the spacers, whereas the membrane was more steady and less vibration occurred. Lu et al. [26] stated that vibration on the film would introduce an extra resistance to the airflow and should therefore be kept to a minimum, to avoid an additional pressure drop.

For the spacer-filled channels, the average pressure drop according to the analyses seems to deviate more than for the empty channel. However, when the airflow is encountering the spacers and enhancing the membrane deflection, the pressure drop will vary more. The affect by the membrane is hard to evaluate in this thesis due to varying results between the supply and exhaust channels and when the occurrence is not consistent regarding the different tests. Thus, an extensive analyses should be conducted before the spacers ability to keep the membranes in place are stated.

8.2.3 Transition to turbulence due to filament

Another aspect that was encountered in the literature, was the local turbulence due to disturbance by the filament. As previously stated, the transition to turbulence flow behind an obstacle depends on the Reynolds number for the overall flow. The Reynolds numbers experimentally evaluated in the present thesis vary between 174 to 348. According to Bird et al. [43], for $Re \approx 100$ vortices will be developed behind the obstacle which creates the “von Kármán vortex street”, which implies the values of this thesis. According to the results obtained in Santos et al. [35] study, the increase of transverse filaments per unit length would accordingly increase the friction factor. However, it is unknown the effect of the chosen mesh screens according to the rapidness of the filaments in this thesis.

Since the local turbulence will affect the friction factor, the effect can be detected on the factor for increasing Re . Woods and Konzable [24] experienced the unsteady flow at a $Re=500$ when the friction factor deviated from the previous pattern and stabilized. According to the present thesis, the stabilization of the friction factor was not obtaining for the evaluated range of Reynolds numbers. In addition, the obtained power regression of the friction factors according to the respective Reynolds numbers were corresponding well to the measured pressure drops. However, according to figure 7.5 given previously, it can be discussed if the flow will soon encounter the local turbulence region due to the friction factor enhancing a more stable pattern. Yet, it would need a more extensive research according to larger Re to obtain for the friction factor has been affected by vortices.

8.3 Pressure drop comparison to other studies

To compare the experimental results regarding the present thesis to other studies, either by the pressure drop or the friction factor was utilized. Which value that will be used for comparison depends on the other study and the information given. The friction factor or pressure drop for this thesis and other studies were given in section 7.3. The average velocities chosen for this thesis, were lower than initiated in other studies. The decision was based on the beneficial influence it would have on the pressure drop. To obtain the wanted airflow rate for ventilation, a larger number of channels would have to be constructed. This would increase the size of the exchanger, which can be an undesirable case when installing in an AHU. Thus, the pressure drop regarding larger airflow rates will have to be evaluated to further ensure low pressure drops and to avoid the increase in size.

According to the study conducted by Liu [20], the pressure drop was used for comparison. The pressure drops obtained in section 7.3.2 showed a great result for the spacers conducted in this thesis. The pressure drops were around 3 and 5 times smaller regarding this study for the worst and best spacer respectively. Since the channel constrictions were identical regarding this and Liu's studies, the deviation in pressure drop seems to have been obtained by the spacers. However, Liu stated that he enhanced a large pressure drop [40] for the experimental testing and would therefore needed further investigation. Thus, the result from this thesis were compared to others.

Further, the friction factors according to Woods and Kozubal [24] spacers regarding the present Reynolds numbers, obtained larger values than according to present spacers which can be seen according to figure 7.5 and 7.6. The tested spacers by Woods and Kozubal obtained friction factors that varied between 1.19 to 4.1 times larger for the lowest to largest deviation regarding the different studies' spacers and the Reynolds numbers. Thus, the improved friction factors varies according to the different spacers obtained by Woods and Kozubal.

The spacers investigated in Woods and Kozubal's study was shown in figure 2.2. From these spacers, the sinusoidal spacer, known as Spacer 2 and (b) for friction factor and figure of the spacers respectively, is the most similar to this thesis spacers. Accordingly, that is the spacer having the most similar friction factor to the current spacers, at least for Test 1-3. Further, these tests have the most similar geometry as Spacer 2. If the friction factor equation for Test 1-3 would have been investigated for larger Re , Spacer 2 might have contributed to a lower friction. However, it is not known if the friction factors for the spacers conducted in this thesis would obtain the same distribution or rather be influenced by transition to turbulence due to the spacer filament. If the friction is not affected, the pressure drop seems to still enhance low pressure drops.

It could be discussed that Test 4-6 obtained a geometry that was somewhat close to Spacer 3. However, the friction factors for Spacer 3 for both attack angels were significantly larger than for the tested spacers in this thesis. A reason for this could be that the tested spacers had a greater ability to keep the membrane steady. Another reason could be the amount of filament inside the channels. However, the porosities were given to be 0.95 - 0.98 [24], which within the same range of the porosities obtained in the present thesis.

Another research that was studied, obtained a significantly low pressure drop through the channels of a flat plate heat exchanger utilizing film as channel separators. Lu et al. [26] achieved a pressure drop between 4.5 to 6 Pa for the average velocity of 1 m/s, whereas this thesis obtained the lowest value of 54 Pa for the same airflow rate. However, no structural support was utilized for the heat exchanger, which has contributed to a larger pressure drop regarding this thesis. Yet, not even the empty channel in this case was close to that value.

As previously given, a common pressure drop through a flat plate heat exchanger for smaller residential buildings can be of approximately 50 Pa [39]. According to this, Test 4 with the 53 Pa for an average velocity of 1 m/s have to possibility to substitute the flat plate heat exchanger. Further, as stated the MEE achieve great sensible and latent efficiencies and if this could be verified for the present spacers, this MEE would be a competition to the conventional heat exchangers.

Conclusions

The present thesis studied the influence of corrugated mesh screens on the pressure drop for an air-to-air membrane energy exchanger. The thesis encountered theoretical and experimental investigation according to the corrugated spacers and the membrane. The pressure drop was experimentally investigated under isothermal conditions, where the efficiency of the exchanger was not evaluated. The structure of the energy exchanger had previously been evaluated and achieved desirable latent and sensible efficiencies for cold climates, hence the same dimensions were chosen for this study.

The experimental conducted testing evaluated the pressure drop over the exchanger concerning spacer-filled and empty channels regarding different airflow rates. Concerning the spacers, six different corrugated mesh screens were experimentally investigated, consisting two corrugated pitches and three mesh screens. Compared to other conducted studies on the field, the result regarding the pressure drop for the spacers showed great potential. Exclusively, one of the investigated spacers enhanced a significantly lower pressure drop. Thus, if the great efficiency of the MEE were still to be obtained when inserting the promising spacer from the present thesis, this exchanger would be promoted as a competition to the conventional heat exchangers utilized in AHUs today.

Additionally, the different evaluated spacers obtained small variation in the porosities. Yet, the experimental pressure drop was clearly affected by the porosity of the spacers. The results gave that the pressure drop regarding the different spacers increased with the reduction in porosity. Regarding the chosen corrugation pitches, the results showed little effect on the porosity, but great influence on the pressure drop. Thus, the influence of the corrugation pitch on the porosity and hence the pressure drop would need an extensive investigation.

The two geometries obtained for the experimental testing spacers, were sinusoidal geometry and a shape more related to rectangle. The latter spacer might have imposed a better ability to keep the membrane in place and from vibrating, but would need further research. Another study has already proven the sinusoidal spacer to sufficiently keep the membrane from deflection.

Concerning the pressure drop investigation, the extensive measurements regarding the pressure taps deviated in the pressure drops according to the same channel. By physical laws, the pressure drop should have been steady over the exchanger. Further, the spacers' ability to keep the membrane steady was hard to evaluate due to varying pressure drop results between the supply and exhaust channels which were not concise regarding the different tests. Thus, an extensive analyses regarding the pressure taps and the pressure drop of the spacers should be conducted before the spacers would have been implemented into exchangers.

In addition, the average velocities obtained in the present thesis were lower than utilized in other studies. The decision was based on the beneficial influence it would have on the pressure drop. To obtain the wanted airflow rate for ventilation, a larger number of channels would have to be installed. This would increase the size of the exchanger, which can be an undesirable case when installing in an AHU. Thus, the pressure drop regarding larger airflow rates will have to be evaluated to further ensure low pressure drops and to avoid the increase in size. However, the pressure drop seems to still enhance low pressure drops compared to other studies.

The use of theoretical comparison should be utilized with care, if not more complicated models appropriate to the spacers would be chosen. Thus, the theoretical calculations were used for selection of corrugation pitches and to better understand how the pressure drop was influenced by increasing airflow rates.

The spacers conducted in this thesis show great promises of reducing the pressure drop through the channels of the membrane energy exchanger and should therefore be further evaluated. A full-scale MEE should be investigated under varying temperatures and over a longer testing period to evaluate durability of the spacers and efficiency.

Chapter 10

Further work

During this master thesis, the experimental test rig was constructed and corrugated spacers were tested in a quasi-counter MEE. However, there are further studies that can be conducted to validate the results or ...

Firstly, multiple spacer for the different testes made in the exact mould and mesh could to ensure that the measured pressure drop was closer to the real value. This would enhance greater certainty to the obtained results and could initiate further validation of the good results. To further reduce the uncertainty, the set of spacers that were created in this thesis could be experimentally tested repeatedly.

Further, moulds could be created for the ramp and sinusoidal spacer respective to corrugation pitch of 10 and 20 mm. Then the influence of the different geometries and corrugation pitches to keep the membrane steady, would be easier to evaluate. In addition, larger corrugation pitches could be investigated to obtain the largest pitch which would still be able to maintain the membrane from deflection. Also, various geometries could be constructed and evaluated to see if others would enhance better ability and reduce the pressure drop.

Moreover, the constructed spacers could have been experimentally investigated for larger Reynolds number whereas the transition to turbulent regime might have occurred. Then a more accurate correlation of the friction factor dependent on the Reynolds number could be obtained. Also, the transition effect due to the filament could be further studied.

Accordingly, to evaluate the influence of the porosity larger deviation of the chosen mesh screens should be chosen. To achieve a greater difference, it might be beneficial if the dimensions are increased of the exchanger channels. This would give the chance to incorporate a broader range of dimension of the wire thickness and mesh size of the screens, whereas the results would be scaled to the appropriate dimensions.

Initially, the spacers were wanted to be tested with to angler area to fit better the to the flow. This will most likely reduce the pressure drop due to less disturbance of the flow and would therefore be of great interest to investigate.

Lastly, the spacers achieving the lowest pressure drop must be evaluated for the sensible and latent effectiveness to ensure that the previously obtained values are still as significant. Thus, a full-size exchanger should be constructed where the efficiencies and pressure drop for cold climates will be investigated. It would also be beneficial to conduct the experiments over a longer time period to ensure durable design of the spacers.

Bibliography

- [1] A. Retterstøl. Design of membrane energy exchanger concerning pressure loss, project work, Norwegian University of Science and Technology. December 2017.
- [2] Core Writing Team, R. K. Pachauri and L. A. Meyer(eds.). *IPCC, 2014: Climate Change 2014: Synthesis Report. Contribution of Working Groups I, II and III to the Fifth Assessment Report of the Intergovernmental Panel on Climate Change*. IPCC, Geneva, Switzerland, 2014.
- [3] SINTEF NTNU. *ENØK i bygninger*. Gyldendal Norsk Forlag AS, ISBN 978-82-05-37496-6, 3 edition, 2007.
- [4] Direktoratet for Byggekvalitet. Byggeteknisk forskrift 17. <https://dibk.no/byggereglene/byggeteknisk-forskrift-tek17/>, 2017.
- [5] P. G. Schild. Nasjonal undersøkelse av boligventilasjon med varmegjenvinning. Research report, Norges byggforskningsinstitutt, 2002.
- [6] Inneklima. Tørr luft. luftfuktighet inne. <http://www.inneklima.com/index.asp?key=RF> access: 24.10.17.
- [7] Peder Wolkoff and Søren K. Kjærgaard. The dichotomy of relative humidity on indoor air quality. *Environment International*, 33(6):850 – 857, 2007.
- [8] S. Ingebrigtsen. *Ventilasjonsteknikk : Del 1*. Skarland press, Oslo, third edition, 2016.
- [9] L. Zhang. Heat and mass transfer in a quasi-counter flow membrane-based total heat exchanger. *International Journal of Heat and Mass Transfer*, 53(23):5478 – 5486, 2010.
- [10] T. Osamu. An analysis of simultaneous heat and water vapor exchange through a flat paper plate crossflow total heat exchanger. *International Journal of Heat and Mass Transfer*, 27(12):2259 – 2265, 1984.
- [11] L. Z. Zhang and J. L. Niu. Effectiveness correlations for heat and moisture transfer processes in an enthalpy exchanger with membrane cores. *Journal of Heat Transfer*, 124(5):922–929, 2002.
- [12] J.L Niu and L.Z Zhang. Membrane-based enthalpy exchanger: material considerations and clarification of moisture resistance. *Journal of Membrane Science*, 189(2):179 – 191, 2001.
- [13] J. Woods. Membrane processes for heating, ventilation, and air conditioning. *Renewable and Sustainable Energy Reviews*, 33:290 – 304, 2014.

BIBLIOGRAPHY

- [14] L.Z. Zhang. Energy performance of independent air dehumidification systems with energy recovery measures. *Energy*, 31(8):1228 – 1242, 2006.
- [15] L.Z. Zhang and Y. Jiang. Heat and mass transfer in a membrane-based energy recovery ventilator. *Journal of Membrane Science*, 163(1):29 – 38, 1999.
- [16] W. M. Kays and A. L. London. *Compact heat exchangers*. Krieger Publishing Company, 1984.
- [17] L.Z. Zhang, X.R. Zhang, Q.Z. Miao and L.X. Pei. Selective permeation of moisture and vocs through polymer membranes used in total heat exchangers for indoor air ventilation. *Indoor Air*, 22(4):321–330, 2011.
- [18] K. L. Wang, S. H. McCray, D. D. Newbold and E.L. Cussler. Hollow fiber air drying. *Journal of Membrane Science*, 72(3):231 – 244, 1992.
- [19] M. Nasif, R. AL-Waked, G. Morrison, and M. Behnia. Membrane heat exchanger in hvac energy recovery systems, systems energy analysis. *Energy and Buildings*, 42(10):1833 – 1840, 2010.
- [20] Peng Liu, Maria Justo Alonso, Hans Martin Mathisen, and Carey Simonson. Performance of a quasi-counter-flow air-to-air membrane energy exchanger in cold climates. *Energy and Buildings*, 119:129 – 142, 2016.
- [21] Peng Liu, Maria Justo Alonso, Hans Martin Mathisen, and Carey Simonson. Energy transfer and energy saving potentials of air-to-air membrane energy exchanger for ventilation in cold climates. *Energy and Buildings*, 135:95 – 108, 2017.
- [22] V. Dvořák and T. Vít. Evaluation of CAE Methods Used for Plate Heat Exchanger Design. *Energy Procedia*, 111:141 – 150, 2017. 8th International Conference on Sustainability in Energy and Buildings, SEB-16, 11-13 September 2016, Turin, Italy.
- [23] R. Al-Waked, M. S. Nasif, G. Morrison and M. Behnia. Cfd simulation of air to air enthalpy heat exchanger. *Energy Conversion and Management*, 74:377 – 385, 2013.
- [24] J. Woods and E. Kozubal. Heat transfer and pressure drop in spacer-filled channels for membrane energy recovery ventilators. *Applied Thermal Engineering*, 50(1):868 – 876, 2013.
- [25] M. D. Larson, R. W. Besant and C. J. Simonson. The effect of membrane deflections on flow rate in crossflow air-to-air exchangers. *HVAC&R Research*, 14(2):275–288, 2008.
- [26] Y. Lu, Y. Wang, L. Zhu and Q. Wang. Enhanced performance of heat recovery ventilator by airflow-induced film vibration (HRV performance enhanced by FIV). *International Journal of Thermal Sciences*, 49(10):2037 – 2041, 2010.
- [27] A. B. Mazo and D. I. Okhotnikov. Local transition to turbulence behind an obstacle for a nominally laminar flow. *Lobachevskii Journal of Mathematics*, 37(3):360–367, May 2016.


- [28] S. K. Karode and A. Kumar. Flow visualization through spacer filled channels by computational fluid dynamics i.: Pressure drop and shear rate calculations for flat sheet geometry. *Journal of Membrane Science*, 193(1):69 – 84, 2001.
- [29] D. E. Wiley J. Schwinge and D. F. Fletcher. Simulation of the flow around spacer filaments between narrow channel walls. 1. hydrodynamics. *Industrial & Engineering Chemistry Research*, 41(12):2977–2987, 2002.
- [30] J. Schwinge, D.E. Wiley, and A.G. Fane. Novel spacer design improves observed flux. *Journal of Membrane Science*, 229(1):53 – 61, 2004.
- [31] C.P. Koutsou, S.G. Yiantsios, and A.J. Karabelas. Direct numerical simulation of flow in spacer-filled channels: Effect of spacer geometrical characteristics. *Journal of Membrane Science*, 291(1):53 – 69, 2007.
- [32] G.A. Fimbres-Weihs and D.E. Wiley. Review of 3d cfd modeling of flow and mass transfer in narrow spacer-filled channels in membrane modules. *Chemical Engineering and Processing: Process Intensification*, 49(7):759 – 781, 2010. Process Intensification on Intensified Transport by Complex Geometries.
- [33] C.C. Zimmerer and V. Kottke. Effects of spacer geometry on pressure drop, mass transfer, mixing behavior, and residence time distribution. *Desalination*, 104(1):129 – 134, 1996.
- [34] A. Subramani, S. Kim, and E. M.V. Hoek. Pressure, flow, and concentration profiles in open and spacer-filled membrane channels. *Journal of Membrane Science*, 277(1):7 – 17, 2006.
- [35] J.L.C. Santos, V. Geraldes, S. Velizarov and J.G. Crespo. Investigation of flow patterns and mass transfer in membrane module channels filled with flow-aligned spacers using computational fluid dynamics (cfd). *Journal of Membrane Science*, 305(1):103 – 117, 2007.
- [36] G. I. Mahmood, C. J. Simonson and R. W. Besant. Experimental pressure drop and heat transfer in a rectangular channel with a sinusoidal porous screen. *Journal of Heat Transfer*, 137(4):042601–1–11, 2015.
- [37] A. Siddiqui, S. Lehmann, V. Haaksman, J. Ogier, C. Schellenberg, M.C.M. van Loosdrecht, J.C. Kruithof, and J.S. Vrouwenvelder. Porosity of spacer-filled channels in spiral-wound membrane systems: Quantification methods and impact on hydraulic characterization. *Water Research*, 119:304 – 311, 2017.
- [38] A S H R A E. *2016 ASHRAE Handbook - Heating, Ventilating, and Air-Conditioning Systems and Equipment (SI Edition)*. American Society of Heating, Refrigerating and Air-Conditioning Engineers, Inc., 2016.
- [39] Danfoss. Air units product datasheet. <https://assets.danfoss.com/documents/DOC234086477844/DOC234086477844.pdf> access: 10.06.18, 2018.

- [40] P. Liu. *Energy Recovery with Air-to-air Membrane Energy Exchanger for Ventilation in Cold Climates*. PhD thesis, Norwegian University of Science and Technology, Norway, 2016.
- [41] Y. A. Cengel and J. M Cimbala. *Fluid Mechanics: fundamentals and applications*. McGrawHill Education, ISBN 978-1-259-01122-1, third edition, 2014.
- [42] R. K. Shah and D. P. Sekulić. *Fundamentals of heat exchanger design*. John Wiley and Sons, Inc., ISBN 0-471-32171-0, first edition, 2003.
- [43] R.B. Bird, W.E. Stewart and E.N. Lightfoot. *Transport phenomena*, 2007.
- [44] R. Chhabra and V.Shankar. *Coulson and Richardson's Chemical Engineering*. McGraw-Hill series in mechanical engineering. Butterworth-Heinemann, seventh edition, 2018.
- [45] S. K. Som and G. Biswas. *Introduction to Fluid Mechanics and Fluid Machines*. Tata McGraw-Hill Publishing Company Limited, revised second edition, 2008.
- [46] Middle East Technical University. Topic 2: Static pressure measurements [lecture notes, powerpoint]. <http://ocw.metu.edu.tr/mod/resource/view.php?id=1127> access: 26.05.18, 2010.
- [47] W. M. Kays and M. E. Crawford. *ASHRAE Handbook: Fundamentals*. American Society of Heating, 2005.
- [48] Matematikknet. Sinusfunksjoner. <http://matematikk.net/side/Sinusfunksjonen> access: 23.10.17.
- [49] L. Lorentzen, A. Hole and T. Lindstrøm. *Kalkulus - med en og flere variable*. Universitetsforlaget, ISBN 978-82-00-42433-8, fourth edition, 2003.
- [50] Wisconsin Geological & Natural History Survey. Understanding porosity and density. <https://wgnhs.uwex.edu/maps-data/data/rock-properties/understanding-porosity-density/> access: 15.03.18, 2018.
- [51] LTD. Anping Bingrong Wire Mesh Products CO. Aluminium-magnesium alloy window screen. <http://www.bingrongironnails.com/pinfo.php?title=Aluminum-magnesium-Alloy-Window-Screen&mid=12&u=668> access: 19.02.18, 2018.
- [52] CT Platon. Glass variable area flowmeres product datasheet. <http://www.ctplaton.com/uploads/pdf/En/deb{ }ng{ }lg.pdf> access: 10.06.18.
- [53] DP Measurement. Tt 570 micromanometer. <https://www.ttseries.com/wp-content/uploads/2017/03/TT-570-Low-Res.pdf> access: 10.06.18.

Appendices

Appendix A

Hazard activity identification process

NTNU	Hazardous activity identification process			Prepared by HSE section	Number HMSRY/2801E	Date 08.01.2018
				Approved by The Rector		Revisions 01.12.2008
HSE						

Unit: Energy and Process Engineering

Line manager: Therese Lovås

Participants in the identification process: Aurora Retterstøl (student), Hans Martin Mathisen (Supervisor), Lars Komrad Sørensen (Rig builder)
 Short description of the main activity/main process: Master thesis for student Aurora Retterstøl. Design of membrane energy exchanger concerning pressure loss.

Is the project work purely theoretical? (YES/NO): NO

Answer "YES" implies that supervisor is assured that no activities requiring risk assessment are involved in the work. If YES, briefly describe the activities below. The risk assessment form need not be filled out.

Signatures: Responsible supervisor: 

Student: Aurora Retterstøl

Date: 15.03.2018

ID nr.	Activity/process	Responsible person	Existing documentation	Existing safety measures	Laws, regulations etc.	Comment
01	Experimental testing different spacers	Aurora Retterstøl	No	No	No	
02	Experimental testing of inlet demo	Aurora Retterstøl	No	No	No	
03	Construction of rig	Aurora Retterstøl	No	No	No	

NTNU	Risk assessment		
	Prepared by HSE section Approved by The Rector	Number HMSRV2603E	Date 04.02.2011 Replaces 01.12.2006

Unit: *Energy and Process Engineering* Date: **15.03.2018**

Line manager: **Therese Lovås**

Participants in the identification process: **Aurora Retterstøl (student), Hans Martin Mathisen (Supervisor), Lars Konrad Sørensen (Rig builder)**

Short description of the main activity/main process: **Master thesis for student Aurora Retterstøl. Design of membrane energy exchanger concerning pressure loss.**

Signatures: *Responsible supervisor: XMM*

Student: Aurora Retterstøl

Activity from the identification process form	Potential undesirable incident/strain	Likelihood (1-5)	Human (A-E)	Environment (A-E)	Economy/material (A-E)	Risk Value (human)	Comments/status Suggested measures
Experimental testing different spacers	Ruin measuring devices	1	A	A	C	1A	Keep track of devices and detach before changing spacers
Experimental testing different spacers	Harm myself on the test rig: pinch finger between plates, cut myself on the spacer	2	B	A	A	2B	Be careful when opening/closing exchanger, be aware of sharp edges on the spacer
Experimental testing of inlet deno	Cut myself on wallpaper knives/scissor	1	B	A	A	1B	Close wallpaper knife/ scissor so sharp blade is not accessible
Construction of rig	Hurt myself on tools	1	B	A	A	1B	Be aware of where tools are and use appropriate protection wear
Construction of rig	Sharp edges on the ductwork	1	B	A	A	1B	Minimize potential of sharp edges by applying ex. Duct tape
Construction of rig	Drop items on toes, getting something into the eyes	1	A	A	A	1A	Wear safety shoes and glasses

Likelihood, e.g.:
1. Minimal
2. Low
3. Medium
4. High
5. Very high

Consequence, e.g.:
A. Safe
B. Relatively safe
C. Dangerous
D. Critical
E. Very critical

Risk value (each one to be estimated separately):
Human = Likelihood x Human Consequence
Environmental = Likelihood x Environmental consequence
Financial/material = Likelihood x Consequence for Economy/material

Potential undesirable incident/strain

NTNU		Prepared by		Number		Date	
		HSE section		HMSRV2603E		04.02.2011	
HSE/IKS		Approved by		The Rector		Revisions	
						01.12.2006	



Risk assessment

Identify possible incidents and conditions that may lead to situations that pose a hazard to people, the environment and any material/equipment involved.

Criteria for the assessment of likelihood and consequence in relation to fieldwork

Each activity is assessed according to a worst-case scenario. Likelihood and consequence are to be assessed separately for each potential undesirable incident. Before starting on the quantification, the participants should agree what they understand by the assessment criteria.

Likelihood	Low 2	Medium 3	High 4	Very high 5
Minimal 1	Once every 10 years or less	Once a year or less	Once a month or less	Once a week

Consequence

Grading	Human	Environment	Financial/material
E Very critical	May produce fatalities/ies	Very prolonged, non-reversible damage	Shutdown of work > 1 year.
D Critical	Permanent injury, may produce serious health damage/sickness	Prolonged damage. Long recovery time.	Shutdown of work 0.5-1 year.
C Dangerous	Serious personal injury	Minor damage. Long recovery time	Shutdown of work < 1 month
B Relatively safe	Injury that requires medical treatment	Minor damage. Short recovery time	Shutdown of work < 1week
A Safe	Injury that requires first aid	Insignificant damage. Short recovery time	Shutdown of work < 1day

The unit makes its own decision as to whether opting to fill in or not consequences for economy/material, for example if the unit is going to use particularly valuable equipment. It is up to the individual unit to choose the assessment criteria for this column.

Risk = Likelihood x Consequence

Please calculate the risk value for "Human", "Environment" and, if chosen, "Economy/material", separately.

About the column "Comments/status, suggested preventative and corrective measures":

Measures can impact on both likelihood and consequences. Prioritise measures that can prevent the incident from occurring; in other words, likelihood-reducing measures are to be prioritised above greater emergency preparedness, i.e. consequence-reducing measures.

NTNU		Risk matrix		prepared by	Number	Date
HSE/KS				HSE Section	HMSRV/2604	8 March 2010
				approved by	Page	Replaces
				Reactor	4 of 4	9 February 2010



MATRIX FOR RISK ASSESSMENTS at NTNU

CONSEQUENCE		E1	E2-	E3	E4	E5
		D1	D2	D3	D4	D5
Moderate		C1	C2	C3	C4	C5
Minor		B1	B2	B3	B4	B5
Not significant		A1	A2	A3	A4	A5
		Very low	Low	Medium	High	Very high
		LIKELIHOOD				

Principle for acceptance criteria. Explanation of the colours used in the risk matrix.

Colour	Description
Red	Unacceptable risk. Measures must be taken to reduce the risk.
Yellow	Assessment range. Measures must be considered.
Green	Acceptable risk. Measures can be considered based on other considerations.

Appendix B

Minor loss coefficients

The minor loss from bends has been given by *ASHRAE* for rectangular ventilation ducts, which is given in table B.1. W is the width and H is the height of the duct, and the ratio of these is called the aspect ratio. [47]

Table B.1: Minor loss values for rectangular bend in ventilation ducts [47]

θ	$K_{L,bend}$ values										
	W/H										
	0.25	0.50	0.75	1.00	1.50	2.00	3.00	4.00	5.00	6.00	8.00
20	0.08	0.08	0.08	0.07	0.07	0.07	0.06	0.06	0.05	0.05	0.05
30	0.18	0.17	0.17	0.16	0.15	0.15	0.13	0.13	0.12	0.12	0.11
45	0.38	0.37	0.36	0.34	0.33	0.31	0.28	0.27	0.26	0.25	0.24
60	0.60	0.59	0.57	0.55	0.52	0.49	0.46	0.43	0.41	0.39	0.38
75	0.89	0.87	0.84	0.81	0.77	0.73	0.67	0.63	0.61	0.58	0.57
90	1.30	1.27	1.23	1.18	1.13	1.07	0.98	0.92	0.89	0.85	0.83

The channel in the MEE is however wider and thinner than a ventilation duct. Therefore, the aspect ratio for a channel in the MEE was too small. Thus, the values from table B.1 were interpolated to find equations most corresponding for all aspect ratios by curve fitting. The series of formulas given in equation B.1 was found to be the most appropriate for different angles on the bends. However, only the equation for 45 ° is relevant for the present thesis and was given in chapter 3.2.2.

$$\begin{aligned}
 K_{L,bend,20^\circ} &= -0.010 \ln x + 0.0718 \\
 K_{L,bend,30^\circ} &= -0.021 \ln x + 0.1574 \\
 K_{L,bend,45^\circ} &= -0.045 \ln x + 0.3356 \\
 K_{L,bend,60^\circ} &= -0.072 \ln x + 0.5338 \\
 K_{L,bend,75^\circ} &= -0.105 \ln x + 0.7887
 \end{aligned}
 \tag{B.1}$$

For the curve fitting equations for $K_{L,bend,i}$ to be used, the aspect ratio noted as x must be calculated as shown in equation B.2.

$$x = \frac{\text{width}}{\text{height}} = \underbrace{\frac{L_{cross}}{H}}_{\text{empty channel}} = \underbrace{\frac{2a_{wave}}{h}}_{\text{Rectangle, triangle and sinusoidal spacer}}
 \tag{B.2}$$

Appendix C

MATLAB-script used in theoretical pressure drop calculations

The MATLAB-script given below has been created and simplified by the author according to previous work [1]. The script contains a code that calculate only the cross-sectional area for the sinusoidal curve

```
1 clear all
2 close all
3 clc
4 w=xlsread('PressureDropCalculation.xlsx','Calc10','B2');
5 h=xlsread('PressureDropCalculation.xlsx','Calc10','B3');
6 n_wave_G=xlsread('PressureDropCalculation.xlsx','General','D36:D42
    ');
7 n_wave_10=xlsread('PressureDropCalculation.xlsx','Calc10','D42');
8 n_wave_20=xlsread('PressureDropCalculation.xlsx','Calc20','D42');
9 n_wave_peng=xlsread('PressureDropCalculation.xlsx','Pengs values',
    'D50');
10
11 b=h/2;
12 A=b;
13
14 %Thesis General
15 n=1;
16 a_G(n)=(w/n_wave_G(n))/2;
17 k_G(n)=pi/a_G(n);
18 y_G=@(x) (A*sin(k_G(n)*x-pi/2)+A);
19 Ac_G(n)=integral(y_G,0,2*a_G(n));
20
21 n=2;
22 a_G(n)=(w/n_wave_G(n))/2;
23 k_G(n)=pi/a_G(n);
24 y_G=@(x) (A*sin(k_G(n)*x-pi/2)+A);
25 Ac_G(n)=integral(y_G,0,2*a_G(n));
26
27 n=3;
28 a_G(n)=(w/n_wave_G(n))/2;
29 k_G(n)=pi/a_G(n);
30 y_G=@(x) (A*sin(k_G(n)*x-pi/2)+A);
31 Ac_G(n)=integral(y_G,0,2*a_G(n));
32
33 n=4;
34 a_G(n)=(w/n_wave_G(n))/2;
```

```

35 k_G(n)=pi/a_G(n);
36 y_G=@(x) (A*sin(k_G(n)*x-pi/2)+A);
37 Ac_G(n)=integral(y_G,0,2*a_G(n));
38
39 n=5;
40 a_G(n)=(w/n_wave_G(n))/2;
41 k_G(n)=pi/a_G(n);
42 y_G=@(x) (A*sin(k_G(n)*x-pi/2)+A);
43 Ac_G(n)=integral(y_G,0,2*a_G(n));
44
45 n=6;
46 a_G(n)=(w/n_wave_G(n))/2;
47 k_G(n)=pi/a_G(n);
48 y_G=@(x) (A*sin(k_G(n)*x-pi/2)+A);
49 Ac_G(n)=integral(y_G,0,2*a_G(n));
50
51 n=7;
52 a_G(n)=(w/n_wave_G(n))/2;
53 k_G(n)=pi/a_G(n);
54 y_G=@(x) (A*sin(k_G(n)*x-pi/2)+A);
55 Ac_G(n)=integral(y_G,0,2*a_G(n));
56
57 Ac_G_inv=Ac_G';
58 xlswrite('PressureDropCalculation.xlsx',Ac_G_inv,'General','E36:
      E42');
59
60 %Thesis P=10mm
61 a_10=(w/n_wave_10)/2;
62 k_10=pi/a_10;
63 y_10=@(x) (A*sin(k_10*x-pi/2)+A);
64 Ac_10=integral(y_10,0,2*a_10);
65
66 xlswrite('PressureDropCalculation.xlsx',Ac_10,'Calc10','E42');
67
68 %Thesis P=20mm
69 a_20=(w/n_wave_20)/2;
70 k_20=pi/a_20;
71 y_20=@(x) (A*sin(k_20*x-pi/2)+A);
72 Ac_20=integral(y_20,0,2*a_20);
73
74 xlswrite('PressureDropCalculation.xlsx',Ac_20,'Calc20','E42');
75
76 %PhD P. Liu
77 a_Liu=(w/n_wave_peng)/2;
78 k_Liu=pi/a_Liu;
79 y_Liu=@(x) (A*sin(k_Liu*x-pi/2)+A);
80 Ac_Liu=integral(y_peng,0,2*a_Liu);
81
82 xlswrite('PressureDropCalculation.xlsx',Ac_Liu,'Lius values','E50'
      );

```

Appendix D

Results of the inlet demonstration

The experiment testing various materials and shapes of diffusion material was conducted to ensure well distributed airflow in the channel. Three materials were tested, two types of *Swix FiberTex*, fine and medium coarse, and lastly regular-density Polyurethane Foam. Different shapes of the materials were tested were presented in chapter 5.1.1 and figure 5.2c. The velocity were measured at three different locations proportional to the cross-sectional area by a VelociCalc. The best solution was selected for the measurements that gave themost uniform velocity over the cross-sectional area.

Figure D.1 shows the construction of the inlet area as well as the measuring locations *a*, *b* and *c*. The velocity was measure for a closed inlet area.

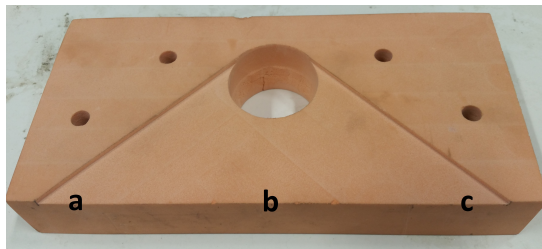


Figure D.1: Location of the different measuring points

The velocity were measure at three different locations as given above. After testing various shapes of the three chosen material as well as an empty inlet area, the results gave closest velocity for the empty area. The velocity through the exchanger will be approximately 1-1.5 m/s dependent on the geometry, and the goal was to be within this range for the current test. The results for the empty inlet area is presenter in reftab:ResultMeasureVelocityInlet by average velocity, \bar{v}_i , for the different measuring locations and respectively the standard deviation.

Table D.1: Velocity and standard deviation for the chosen diffusion pieces at the end of the inlet area

	a		b		c	
	\bar{v}	σ	\bar{v}	σ	\bar{v}	σ
Empty	2.36	0.0265	1.81	0.0129	2.20	0.0263

As the result show, the velocity variation was as relatively low and quite stable over the whole cross-sectional area, but was not within the expected range. Unfortunately, lower velocities was not able to reach when the lowest rotational speed on the fan was used. However, if calculating the Reynolds number to be less than 1120 for the largest velocity, 2.36 m/s , the flow is still laminar.

To avoid uncertainty according to the VelociCalc, the same instrument was used for all measurements. The error in the instrument has been considered to be equal for all measurements. Since the velocity in particular is not interesting where as the uniformly air distribution is, the error due to the instrument is neglected.

Appendix E

Specific values for the created moulds

The moulds were used to corrugate the mesh screen into spacers. Thus, more specific values regarding the two moulds that were created in the present thesis are given in table E.1.

Table E.1: Specific properties of the moulds

Mould	Corrugation pitch [mm]	Height [mm]	Apex angle [°]	Width [m]	Length [m]	Number of waves [-]
1	10	5	90	0.27	0.7	27
2	20	5	-	0.27	0.7	9

Appendix F

Specific values for the measurement schedule

According to the measurement schedule given in section 5.3, a more detailed information about the testes and corrugated mesh screens are given in table F.1.

Table F.1: Specific values for the measurement schedule

Test	Wire thickness [mm]	Mesh size [mm x mm]	Corrugation pitch [mm]	Apex angle [°]	Number of waves [-]
0	-	-	-	-	-
1	0.2	2.00 x 1.68	10	136 - 9	25
2	0.22	1.41 x 1.41	10	136 - 9	25
3	0.22	1.19 x 1.19	10	136 - 9	25
4	0.2	2.00 x 1.68	20	-	8.3
5	0.22	1.41 x 1.41	20	-	8.3
6	0.22	1.19 x 1.19	20	-	8.3

Appendix G

Parameters obtained by the porosity calculation of the corrugated mesh screens

Before the porosity could be found, other relations had to be calculated. According to the equations stated in section 4.2, the calculated values are stated in table G.1.

Table G.1: Parameters needed to calculate the porosity of the corrugated mesh screens

Test	n_{waves} [-]	α [°]	$L_{y,wire}$ [mm]	$L_{x,wire}$ [mm]	A_{wire} [mm ²]	V_{wire} [mm ³]	σ [%]
1	25	1.19	70.7	78.3	0.0314	4.67×10^3	0.982
2	25	1.19	100.3	93.1	0.0380	7.35×10^3	0.972
3	25	1.19	118.8	110.3	0.0380	8.71×10^3	0.967
4	8.3	1.19	67.3	78.1	0.0314	4.57×10^3	0.983
5	8.3	1.19	95.5	93.1	0.0380	7.17×10^3	0.973
6	8.3	1.19	113.1	110.3	0.0380	8.49×10^3	0.968

Appendix H

Pressure drop theoretical calculation

The theoretical calculated pressure drop was conducted in the manner described in chapter 3 and 1.5, and the pressure drop results are stated below for the different calculations.

Calculation of the empty channel

Since the calculated pressure drop through the exchanger does not depend on different spacers, the result of the calculated pressure drop for different airflow rates are stated in table H.1.

Table H.1: Theoretical pressure drop calculated for the different geometries

Airflow rate [L/min]	ΔP [Pa]
20	24.6
25	30.9
30	37.3
35	43.7
40	50.2
45	56.7
50	63.3

Varying corrugation pitch

The pressure drop was first calculated for the different geometries for varying corrugation pitches. This was done to be able to choose corrugation pitches that would be experimentally tested. The result for the varying corrugation pitches is given in table H.2 for an airflow rate of 30 L/min.

Table H.2: Theoretical pressure drop calculated for the different geometries at 30 L/min

Corrugation pitch [m]	ΔP [Pa]	
	Sinusoidal	Ramp
0.05	71.0	39.0
0.03	72.5	39.7
0.02	74.6	40.6
0.015	77.1	41.5
0.01	82.9	43.4
0.008	87.9	44.9

Varying airflow rate

The pressure drops varying with the airflow rates for the chosen corrugation pitches are given below. First is the pressure drop for the corrugation pitch of 10 mm stated in table H.3. Then, table H.4 stated the pressure drop results for the corrugation pitch of 20 mm.

Table H.3: Theoretical pressure drop for the different geometries according to a corrugation pitch of 10 L/min

Airflow rate [L/min]	ΔP [Pa]	
	Sinusoidal	Ramp
20	54.7	28.3
25	68.7	35.8
30	82.9	43.4
35	97.2	51.1
40	111.7	59.0
45	126.3	67.1
50	141.1	75.2

Table H.4: Theoretical pressure drop for the different geometries according to a corrugation pitch of 20 L/min

Airflow rate [L/min]	ΔP [Pa]	
	Sinusoidal	Ramp
20	49.2	26.4
25	61.8	33.5
30	74.6	40.6
35	87.6	47.9
40	100.6	55.3
45	113.9	62.8
50	127.2	70.5

Appendix I

Results of the pressure drop from actual experiments

The pressure drop results according to the experimental testing is given in this section. First, the average pressure drop regarding all tests are stated in table I.1.

Table I.1: The average pressure drop for the exchanger for the different conducted tests

		Airflow [L/min]		
		20	30	40
$\Delta\bar{P}$ [Pa]	Test 0	26	40	54
	Test 1	44	77	114
	Test 2	46	80	119
	Test 3	47	83	124
	Test 4	31	53	78
	Test 5	35	63	95
	Test 6	36	64	96

Further, the statical pressure drops were obtained at different pressure taps perpendicular to the channel wall and was denoted by the letters from a-f, shown in figure I.1, regarding whether the taps were located at the supply or exhaust channel, as previously explained. Thus, these pressure drop at the different taps are stated in the sections below for the different tests.

Regarding the different tests, two assessments were conducted which were denoted I and II. According to the empty channel, these represented different measurements conducted to the channel. As for the spacer-filled channels, the different assessments described the two pairs of spacers conducted for the same test. Correspondingly, different analyses were conducted for the investigated assessments, whereas the analyses were dependent on the location of where the air was being supplied into the channels. These have been named N (Normal) and T (Turned). Regarding the empty channel, the air was supplied to both ends of Channel B, to investigate if there were any pressure differences between the flow directions through the channel.

For the tables below, table I.2, I.3, I.4, I.5, I.6, I.7 and I.8 respectively belongs to Test 0, Test 1, Test 2, Test 3, Test 4, Test 5 and Test 6. The notations given in the tables have a common meaning, which is stated below.

- \dot{V} The airflow rate
- i The assessment
- j The analyses
- φ The differential pressure drop regarding the different channels for the same analysis
- $\Delta \bar{P}_j$ The average pressure drop over all pressure taps for the same analyses
- $\Delta \bar{P}_i$ The average pressure drop according the assessment

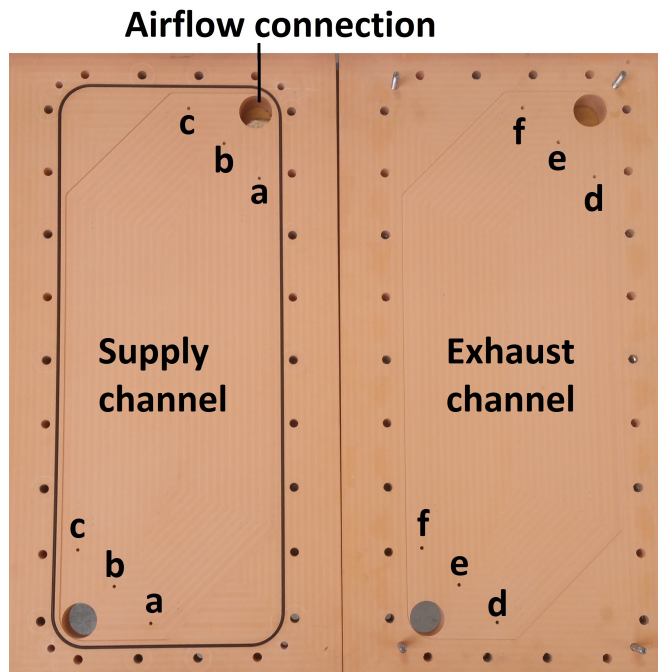


Figure I.1: Notation of pressure taps in the exchanger (regiven)

Empty channel

Test 0 - Channel without spacers

The pressure drop for the empty channel was measured only for Channel B. Thus, i represents the different times the empty channel was measured and j the way the air flow through the channel. Further, since only one channel were investigated, there were only three taps that were utilized. Also, the differential pressure drop regarding different channels were then excluded.

Table I.2: The pressure drop according to the different pressure taps for Test 0. The average pressure drop for different measurements are also given

\dot{V} [L/min]	i	j	Pressure taps [Pa]			$\Delta\bar{P}_j$	$\Delta\bar{P}_i$
			a	b	c	[Pa]	[Pa]
20	I	N	24	29	27	27	27
		T	25	29	26	27	
	II	N	25	28	25	26	26
		T	24	29	25	26	
30	I	N	36	45	43	41	41
		T	39	46	39	41	
	II	N	39	40	39	39	39
		T	35	41	39	38	
40	I	N	48	61	59	56	56
		T	52	62	53	56	
	II	N	53	56	54	54	53
		T	46	55	52	51	

Tested corrugated mesh screens

According to the spacer-filled channels, channel A and B were both investigated as supply and exhaust channels. When Channel A was conducted as the supply channels it was denoted N and T for Channel B. Thus, the spacers inserted into the various channels could both be evaluated for the effects of being either inside the supply or exhaust channel. Further, the first pair of spacers (I) were experimentally investigated twice. After the first conducted measurements, the spacers were reinserted into the channels and investigated according to the same procedure as stated above. This was accomplished so the results would minimize constructional errors and uncertainties when the exchanger was reassembled. The pressure drop results were averaged according to the same assessment since it was the same pair of spacers that were investigated.

Lastly, the second pair of spacers (II) were created with the same mesh screens and moulds for the respective tests. This was conducted to ensure that the average pressure drop was durable for more than one set of identical spacers. These tests were conducted in the same manner as described above, but only measured once due to time limit. However, Test 6 was only conducted once and is therefore lacking *II*.

Further, φ states the difference in pressure drop according to the different channels for the same test (*i*). The larger the difference is, the larger deviation in the results according to the set regarding two different tested spacers.

Test 1 - Mould 1 and Mesh I

Table I.3: The pressure drop according to the different pressure taps for Test 1. The average pressure drop for different measurements are also given

\dot{V} [L/min]	i	j	Pressure taps [Pa]						φ [Pa]	$\Delta\bar{P}_j$ [Pa]	$\Delta\bar{P}_i$ [Pa]
			a	b	c	d	e	f			
20	I	N	26	31	27	56	63	54	30	43	43
		T	54	61	54	28	32	27	-27	42	
	II	N	26	33	30	63	69	59	34	47	45
		T	48	54	45	36	44	37	-10	44	
30	I	N	45	52	47	98	128	94	54	74	74
		T	92	105	95	50	57	47	-46	74	
	II	N	43	55	50	113	125	105	65	82	80
		T	81	92	76	67	81	66	-12	77	
40	I	N	65	77	68	147	169	141	82	111	110
		T	134	154	136	76	85	69	-65	109	
	II	N	60	78	71	171	187	157	102	121	117
		T	115	131	110	102	124	100	-10	114	

Test 2 - Mould 1 and Mesh II

Table I.4: The pressure drop according to the different pressure taps for Test 2. The average pressure drop for different measurements are also given

\dot{V} [L/min]	i	j	Pressure taps [Pa]						φ [Pa]	$\Delta\bar{P}_j$ [Pa]	$\Delta\bar{P}_i$ [Pa]
			a	b	c	d	e	f			
20	I	N	50	59	54	45	53	43	-7	50	51
		T	40	48	42	56	65	59	17	51	
	II	N	42	46	41	39	45	38	-2	42	41
		T	36	43	37	43	47	39	4	41	
30	I	N	85	100	91	79	95	75	-9	87	88
		T	67	81	69	100	117	103	35	89	
	II	N	72	81	70	69	82	66	-2	73	72
		T	62	75	67	76	83	65	7	71	
40	I	N	120	143	131	117	143	113	-7	128	130
		T	95	117	101	151	179	155	57	133	
	II	N	105	121	103	102	122	99	-2	128	107
		T	89	108	98	113	124	98	13	105	

Test 3 - Mould 1 and Mesh III

Table I.5: The pressure drop according to the different pressure taps for Test 3. The average pressure drop for different measurements are also given

\dot{V} [L/min]	i	j	Pressure taps [Pa]						φ [Pa]	$\Delta\bar{P}_j$ [Pa]	$\Delta\bar{P}_i$ [Pa]
			a	b	c	d	e	f			
20	I	N	50	55	51	49	57	46	-2	51	51
		T	46	55	47	53	59	51	5	52	
	II	N	36	39	33	48	56	44	13	43	43
		T	46	52	45	39	42	33	-10	43	
30	I	N	86	97	87	87	102	8	0	90	90
		T	79	95	82	94	104	91	11	91	
	II	N	63	68	58	87	99	78	25	76	76
		T	80	94	81	71	75	57	-17	76	
40	I	N	125	141	126	132	155	122	5	133	134
		T	116	140	120	143	159	137	21	136	
	II	N	91	102	86	133	152	118	41	114	114
		T	118	139	119	109	115	85	-22	114	

Test 4 - Mould 2 and Mesh I

Table I.6: The pressure drop according to the different pressure taps for Test 4. The average pressure drop for different measurements are also given

\dot{V} [L/min]	i	j	Pressure taps [Pa]						φ [Pa]	$\Delta\bar{P}_j$ [Pa]	$\Delta\bar{P}_i$ [Pa]
			a	b	c	d	e	f			
20	I	N	23	29	24	31	37	24	5	28	29
		T	23	33	26	30	36	28	4	29	
	II	N	38	45	40	20	27	18	-19	31	33
		T	16	22	18	49	53	45	30	34	
30	I	N	37	48	39	57	66	42	13	48	50
		T	38	55	43	57	65	51	12	51	
	II	N	62	74	64	36	51	32	-27	53	56
		T	25	37	29	87	96	80	57	59	
40	I	N	50	65	53	89	101	63	29	70	73
		T	53	79	59	88	100	79	25	76	
	II	N	82	100	87	55	78	50	-29	75	82
		T	34	51	40	137	149	123	95	89	

Test 5 - Mould 2 and Mesh II

Table I.7: The pressure drop according to the different pressure taps for Test 5. The average pressure drop for different measurements are also given

\dot{V} [L/min]	i	j	Pressure taps [Pa]						φ [Pa]	$\Delta\bar{P}_j$ [Pa]	$\Delta\bar{P}_i$ [Pa]
			a	b	c	d	e	f			
20	I	N	41	47	39	30	40	26	-10	37	37
		T	20	32	24	46	54	44	23	36	
	II	N	29	38	32	29	38	31	0	33	34
		T	25	35	31	41	43	33	9	35	
30	I	N	69	79	66	61	77	48	-9	66	66
		T	33	54	40	84	102	79	46	65	
	II	N	50	64	53	52	68	56	3	57	60
		T	43	59	53	79	81	60	22	63	
40	I	N	97	112	95	104	124	79	1	102	101
		T	46	77	55	134	164	126	82	100	
	II	N	70	91	75	79	105	85	11	84	89
		T	60	84	75	125	127	91	41	94	

Test 6 - Mould 2 and Mesh III

Table I.8: The pressure drop according to the different pressure taps for Test 6. The average pressure drop for different measurements are also given

\dot{V} [L/min]	i	j	Pressure taps [Pa]						φ [Pa]	$\Delta\bar{P}_j$ [Pa]	$\Delta\bar{P}_i$ [Pa]
			a	b	c	d	e	f			
20	I	N	36	46	41	25	34	24	-13	34	36
		T	19	29	24	47	54	47	25	38	
30	I	N	60	77	69	46	64	45	-17	60	64
		T	32	51	43	89	102	87	51	67	
40	I	N	84	109	98	71	100	70	-17	89	96
		T	45	75	61	144	163	134	87	104	